Climate Dynamics
https://doi.org/10.1007/s00382-024-07380-2

ORIGINAL ARTICLE

MJO-equatorial Rossby wave interferences in the tropical intraseasonal oscillation

Yuntao Wei[1,2,3] · **Hong-Li Ren**[2,4] · **Wansuo Duan**[3] · **Guodong Sun**[3]

Received: 22 March 2024 / Accepted: 23 July 2024
© The Author(s), under exclusive licence to Springer-Verlag GmbH Germany, part of Springer Nature 2024

Abstract
A better understanding and simulation of the tropical intraseasonal oscillation (ISO) is the cornerstone of subseasonal-to-seasonal predictions. Here, we have revealed crucial roles of interference effects between Madden–Julian Oscillation (MJO) and low-frequency equatorial Rossby (ER) waves on the intensity, structure and initiation of the ISO. Over where ER waves are sufficiently strong, the ISO convection usually manifests localized strengthening or weakening due to constructive or destructive MJO-ER interferences. For the ISO interannual variability, though the strength is determined by the MJO, the area is largely controlled by ER waves. The Maritime Continent MJO (ER) varies synchronously (asynchronously) with El Niño-Southern Oscillation likely controlled by the meridional mean moisture gradient. Additionally, separating MJO and ER components helps explain the northwest-southeast tilted structure of boreal summer ISOs, which dramatically arises from decreased phase speeds of the MJO away from the equator. Moreover, the considerable damping of ISO deep convection over the Maritime Continent partly arises from the further weakened MJO aloft due to the dry intrusion of ER waves triggered from the central-eastern Pacific. Finally, a primary ISO event with jumping-like propagation behaviors is likely initiated over the Indian Ocean with the strengthening of preceding ER waves, implying a novel "initiation-propagation" linkage of the ISO. These ER signals may be detected approximately 20 days ahead from the western Pacific and are thus potentially useful for monitoring and predicting ISO initiation early. Taking together, the findings here highlight the importance of ER waves in understanding the dynamics and predictability of the ISO/MJO.

Keywords Madden–Julian Oscillation · Equatorial Rossby wave · Wave interferences · Maritime Continent barrier · El Niño

✉ Yuntao Wei
yuntao_wei@fudan.edu.cn

✉ Hong-Li Ren
renhl@cma.gov.cn

1 CMA-FDU Joint Laboratory of Marine Meteorology, Department of Atmospheric and Oceanic Sciences and Institute of Atmospheric Sciences, Shanghai Frontiers Science Center of Atmosphere-Ocean Interaction, Fudan University, Shanghai 200438, China

2 Collaborative Innovation Center on Forecast and Evaluation of Meteorological Disasters (CIC-FEMD), Nanjing University of Information Science and Technology, Nanjing 210044, China

3 LASG, Institute of Atmospheric Physics, Chinese Academy of Sciences, Beijing, China

4 State Key Laboratory of Severe Weather, and Institute of Tibetan Plateau Meteorology, Chinese Academy of Meteorological Sciences, Beijing, China

1 Introduction

1.1 The tropical intraseasonal oscillation

Tropical winds, cloudiness and rainfall manifest significant fluctuations on the intraseasonal time scale with a broad period range of 20–100 days (Zhang 2005). These signals of the intraseasonal oscillations (ISO) can manifest as eastward and/or westward wave envelopes and even a non-propagating mode (Wang and Rui 1990; Zhang and Hendon 1997; Wang et al. 2019). The pulse-like, episodic ISO events usually start from the Indian Ocean and can be preconditioned by diverse precursor signals (Matthews 2008; Takasuka and Satoh 2021; Wei et al. 2023a, b). If treated as a wave phenomenon, the ISO mainly consists of two well-defined modes, namely the eastward-propagating Madden–Julian Oscillation (MJO; Madden and Julian 1971, 1972) and the westward-propagating equatorial Rossby (ER) waves (Kiladis et al. 2009).

Published online: 05 August 2024

The eastward-propagating MJO mode reaches its annual maximum during boreal winter (Madden 1986; Zhang and Dong 2004), while it becomes weak and the northward propagation mode emerges during boreal summer (Kikuchi 2021). Zhang et al. (2020) compared four popular theories of the MJO, including the multiscale "skeleton" model (Majda and Stechmann 2009, 2011), the "moisture mode" theory (Sobel and Maloney 2013; Adames and Kim 2016; Adames and Maloney 2020), the gravity wave model (Yang and Ingersoll 2013, 2014) and the trio-interaction theory (Wang et al. 2016). Recently, the MJO theories are further developed with several new mechanisms or feedbacks proposed, such as the key role of the meridional moisture advection (Ahmed 2021; Wang and Sobel 2022; Wei and Ren 2024), the dry dynamics (Kim and Zhang 2021; Rostami et al. 2022) or the temperature feedback (Chen 2022a; Mayta and Adames 2023) and a "minimal" mechanism named the wind-evaporation feedback (Mamidi and Mathew 2023). Note that these theories have been developed to exclusively simulate a slowly eastward-propagating, MJO-like mode with a planetary-scale instability.

The ER wave has received less attention in previous studies, as compared to the MJO. The characteristics of the ER wave may change with the longitude. Over the Western Hemisphere, for example, the ER wave propagates westward fast (~ 17 m/s) and displays a vertically barotropic, equatorially symmetric structure (Kiladis and Wheeler 1995; Wheeler and Kiladis 1999) like the dry mode of Matsuno (1966). In contrast, over the Indo-Pacific warm pool, the ER wave is largely asymmetric about the equator, with a slow westward propagation speed (~ 5 m/s) and a baroclinic structure (Wheeler et al. 2000; Yang et al. 2007a, 2007b; Kiladis et al. 2009). Although the easterly vertical wind shear was previously emphasized as a destabilizing factor of baroclinic ER waves (Wang and Xie 1996; Xie and Wang 1996; Chen 2022b), the thermodynamical processes related to the moisture, fluxes and convection might also support the unstable growth of ER waves (Nakamura and Takayabu 2022). Recently, some studies even suggested the low-frequency ER wave as a "moisture mode" (Adames et al. 2019; Mayta et al. 2022) or a "WISHE-moisture mode" (Emanuel 1987; Fuchs and Raymond 2017; Fuchs et al. 2019; Chen 2022b). In this framework, the ER wave is destabilized by wind-evaporation and cloud-radiation feedbacks like the MJO. But unlike the MJO propagated mainly by the meridional moisture advection, the propagation mechanisms of slow ER waves emphasize the crucial role of the zonal moisture advection, as the meridional moisture advection retards the westward propagation of ER waves (Gonzalez and Jiang 2019).

Despite considerable progress in the theoretical understanding of MJO and ER waves, numerical climate models are still struggling to simulate fundamental characteristics of ISO modes, such as the primary initiation of MJO events (Matthews 2008) and the northwest-southeast tilted rain band of boreal summer ISO (Neena et al. 2017; Konda and Vissa 2022). Additionally, climate models usually exaggerate the "damping effect" of the Maritime Continent (MC) on the MJO (Kim et al. 2016, 2019; Zhang and Ling 2017), which tends to be reduced in current versions of climate models (e.g., Ahn et al. 2020; Chen et al. 2022), though debates remain (Le et al. 2021). This reflects that underlying mechanisms of the MJO minimizing over the MC are still elusive, although the complex MC topography might dampen the MJO due to friction (Sobel et al. 2008) and competing effects of the land diurnal cycle (Ling et al. 2019). Because the MJO is a major predictability source on the time scale from 2 weeks to 2 months (Waliser et al. 2003; Neena et al. 2014), a poor simulation of the MJO hinders skillful subseasonal predictions of weather and climate extrema, such as tropical cyclones, flooding and heatwaves (Zhang 2013). Therefore, it is of great importance to thoroughly investigate the initiation, organization and propagation dynamics of the MJO/ISO. Although aforementioned studies targeted the MJO, many of them have explored the convective-circulation evolution features of the total ISO that also include the westward ER component.

1.2 Interferences between MJO and ER wave modes

Based on previous studies, MJO and ER wave modes involve considerable interactions (e.g., Roundy and Frank 2004a, b, hereafter RF04b). For example, through the regression upon an MJO-filtered index of the convection over the South Indian Ocean (10° S, 90° E), RF04b found that the ER wave can be enhanced in convection active phases of the MJO while reduced in suppressed phases. Moreover, due to dynamical reflection effects, the ER wave mode might change to an eastward-propagating mode over the East African Highlands, thereby facilitating the MJO initiation (Wei et al. 2019). However, when the MJO encounters the Andes over South America, it might become an ER wave that propagates westward into the western Pacific and even further into the Indian Ocean. Therefore, including the ER wave mode and figuring out its interference mechanisms with the MJO should advance our understanding of the fundamental dynamics of the ISO and thus improve the subseasonal prediction skills of extreme weather and climate in tropical and extratropical regions (Gloeckler and Roundy 2013; Roundy 2023).

Firstly, the ISO propagation and its diversity may be well explained by the ER wave interfering with the MJO. RF04b revealed that the standing ISO exists at the highland regions of East Africa and the west coast of South America, owing to the regional strengthening or suppression of the intraseasonal convection under intersections of MJO and ER waves. Unfortunately, RF04b only considered one base point over

the South Indian Ocean during boreal winter, whether considerably strengthened or weakened convection exists locally elsewhere over the Indo-Pacific warm pool and potential influences of seasonal variations are still unclear. In a recent study by Wei et al. (2023b), they discovered distinct roles of MJO and ER wave modes in shaping the ISO diversity of zonal propagation (Wang et al. 2019). Specifically, the ISO crossing through the MC barrier is primarily preconditioned by a dry MJO phase over the western Pacific, and a further enhancement of the western Pacific suppressed convection due to the dry intrusion of the ER wave can speed up the ISO. Without the ER wave intrusion, however, the ISO's speed might become small. More interestingly, the strengthening or weakening of ER waves can even shape the jumping and standing ISOs when the dry MJO convection is weak over the western Pacific. Huang and Pegion (2022) also found stronger ER wave signals in the jumping ISO than in the standing ISO, though they did not extract and examine the ER wave mode explicitly from diverse ISO propagations.

Secondly, the ER wave mode might explain the initiation of the ISO moist convection. Among others, Wei et al. (2019, 2020) revealed that the conditional nonlinear optimal perturbation (Mu et al. 2003) of moisture, which behaves as an ER wave-like mode, can effectively trigger a strong primary event in a hybrid atmosphere–ocean coupled model. Through observational analysis, they also found that roughly half of primary events were preconditioned by ER wave-like disturbances from the eastern Indian Ocean. Besides the Indian Ocean, the ER wave signal may also breed from the tropical Pacific (e.g., Feng and Li 2016; Li et al. 2022). Takasuka and Satoh (2021), for example, suggested that the ER wave from the central-eastern Pacific can trigger the onset of ISO deep convection over the western Pacific. Komaromi et al. (2019) revealed that the onset of the December 2011 ISO event can be well forecasted more than 3 weeks in advance when the ER wave traveling from the central Pacific to the Indian Ocean during November 2011 can be captured. More recently, Wei et al. (2023a) documented four types of ISO initiation precursor signals through a clustering analysis. A key finding of their work was the robust extraction of a new mechanism of primary initiation with the help of ER wave signals 30–40 days ahead from the central Pacific. Such an ER wave signal increases the predictability of the primary convective initiation by 1 week compared to other primary events without preconditioning effects of ER waves.

1.3 Synthesis

We have been used to examining the ISO through only bandpass filtering (such as 20–100 days). However, the filtered anomalies consist of eastward-propagating MJO and westward-propagating ER waves involving complex interactions. We might not fully understand the paradigm of the ISO initiation, structural organization and propagation, and thus skillful predictions of extreme events with a time horizon of 2 weeks to two months may not be obtained if we ignore the ER wave and its interference with the MJO mode. Although large efforts have been made to target mechanisms of MJO-ER wave interactions, some fundamental issues are still to be addressed. For example, what are the distinct contributions of MJO and ER wave modes to the ISO, and are there some regionality and seasonality (Masunaga 2007; Yasunaga 2011)? How will the MJO interfering with the ER wave impact the ISO convective structure? Moreover, from previous studies, the ER wave tends to be crucial in the primary convective initiation (Feng and Li 2016; Wei et al. 2023a). So, what are the relative roles of ER waves in the initiation of primary and successive events? Are the former preconditioned by ER wave signals more frequently than the latter?

With these questions in mind, we give the arrangement of the rest of this paper as follows. Section 2 introduces the data and methodology. Section 3 represents the main results of this study, with a particular emphasis on documenting the role of ER waves in explaining the ISO strength, structure and initiation from the Indian Ocean. Section 4 discusses and summarizes our main findings.

2 Data and methods

2.1 Data, pre-processing and definitions

The main dataset used in this study is the daily, 2.5°×2.5°, advanced very high-resolution radiometer outgoing longwave radiation (OLR) during 1979–2018 from the National Oceanic and Atmospheric Administration (NOAA; Liebmann and Smith 1996). Before any filtering operations, we first calculate daily anomalies by subtracting the calendar daily climatology (Waliser et al. 2009). Intraseasonal circulation signals, such as anomalous winds and humidity, are diagnosed using the fifth generation of ECMWF reanalysis products (Hersbach et al. 2020). Additionally, the real-time multivariate MJO (RMM) index (Wheeler and Hendon 2004; Ren et al. 2023) and OLR-based MJO index (OMI; Kiladis et al. 2014) are also used here. We measure the El Niño-Southern Oscillation (ENSO) using the Niño3.4 index, which is calculated as the three-month running mean of sea surface temperature (SST) anomalies over (120°–170° W, 5° N–5° S) using the monthly global 2°×2° Extended Reconstructed SST version 5 (Huang et al. 2017).

Using the Lanczos filter with 201 weights, we perform the 20–100-day bandpass filtering on daily anomalies to extract the ISO, which naturally includes eastward and westward wave components. The "space–time filtering" method (Wheeler and Kiladis 1999) is further used to isolate these

two wave components. Firstly, the Fast Fourier Transform (FFT) is performed along each latitude of 30° S–30° N and then along the time. Secondly, the inverse FFT is performed to retrieve specific wave components constrained by three key parameters, i.e., period, zonal wavenumber and equivalent depth (Table S1). For example, the MJO mode is extracted by retaining only Fourier components of eastward zonal wavenumbers 0–30 and period range of 20–100 days. The same procedures are also used to extract the ER mode, except for considering westward zonal wavenumbers 1–30 and equivalent depth range of 0–1000 m. Note that we have set a broader range of zonal wavenumbers used in the filtering procedure to sufficiently include eastward- and westward-propagating intraseasonal modes, and also to well reconstruct the total ISO. Besides, the "ER wave" defined here is more related to low-frequency, high-order Rossby waves (Wang et al. 2022).

The ISO strength in each grid point is defined as the standard deviation (STD) of the daily, 20–100-day filtered OLR time series in a prescribed month or a month period. For example, to resolve the seasonal cycle of the ISO strength in a year, we have calculated the STD in each calendar month. To derive the interannual variability, we first calculate the STD of the ISO in running windows of 3 months in each grid point. Then, the monthly climatology of the STD is subtracted from the raw STD time series to obtain monthly anomalies of the ISO strength. The above definitions and calculations are further repeated for MJO and ER wave modes to separately define their strength.

2.2 The regression and composite analysis

To diagnose the general impacts of MJO and ER waves on the zonal propagation and horizontal structures of the ISO, we derive a reference time series as the averaged OLR anomaly of the ISO in such an area where the ER/MJO ratio is large (e.g., > 0.5). The OLR anomalies of ISO, MJO and ER waves are then regressed upon the reference time series. Note that our diagnostic procedures are distinct from RF04b who only focused on ER waves that directly correlate with eastward-filtered MJO indices. In contrast, the base index defined here includes both eastward and westward-moving signals no matter whether they correlate with the eastward-moving MJO signal or not. Regressing filtered ER or MJO data against the combined index will yield all ER and MJO signals associated with the eastward and westward filtered base index. Therefore, our results will include ER wave signals that were directly excluded from RF04b. The method here has examined all ER wave signals, including those uncorrelated with the eastward-moving MJO signal, and it addresses partially unrelated questions to those studied by RF04b.

To examine how MJO-ER wave interferences influence the ISO initiation, we construct an index as the averaged OLR anomaly of the ISO over the equatorial Indian Ocean (15° S–15° N, 70°–100° E). The initiation of the ISO is identified when the index becomes smaller than one negative STD. The first day of these consecutive days is labeled "Day 0". In this way, we selected 238 events from 1979 to 2018, implying roughly six events of ISO initiation each year. As expected from the index definition, the distribution of OLR anomalies for the total ISO across all Day 0 is narrowly regular and centered on approximately − 12.0 W/m^2 (Fig. 1a). In contrast, both MJO and ER waves display a considerable scatter, which allows us to classify the impacts of MJO-ER wave interferences on the ISO initiation under different scenarios. Although the averaged ER wave is a bit weaker than the MJO, the former can be stronger than the latter in many cases (Fig. 1c). Moreover, in the equatorial Indian Ocean, the ER wave signal is negatively correlated (approximately − 0.75) with the MJO convection (Fig. 1d). This is likely expected, as the MJO + ER tends to mimic the total ISO. Actually, the former is significantly correlated (~ 0.42) with the latter in terms of OLR anomalies on Day 0. On other lag days, the correlation even exceeds 0.9 (Fig. 1b). Thus, the MJO + ER is a good proxy of the total ISO for selected events (see individual cases in Fig. S1).

In this regard, the cases of the ISO initiation can be grouped by only considering the strength of such as the ER wave. Based on the mean and half of the STD of the ER wave convection across all ISO events, we have defined three scenarios: Weak ER, Moderate ER and Strong ER, in which the ER wave strength increases while the MJO strength decreases gradually (see the large-size circle markers in Fig. 1d). Thus, three groups of composite for the ISO initiation are obtained and we compare the spatiotemporal evolutions of ISO, MJO and ER waves.

3 Results

3.1 The *ISO* strength

The ISO strength shows an evident seasonal variation and generally maximizes in the Summer Hemisphere (Fig. 2a, f). The STD patterns of MJO + ER well fit the ISO (Fig. 2b, g), again suggesting that we might understand the ISO seasonality and regionality by quantifying the relative contributions of MJO and ER wave modes. During boreal summer (May to October), the maximum of the ISO over the Indian Ocean is mainly contributed by the MJO mode (Fig. 2c), to which the ER's contribution is comparable (Fig. 2d). In contrast, over the Northwest Pacific, the ISO is dominated by the ER wave (Fig. 2e). During boreal winter (November to April), the ISO detours via the southern MC (Fig. 2f) mainly due to the MJO

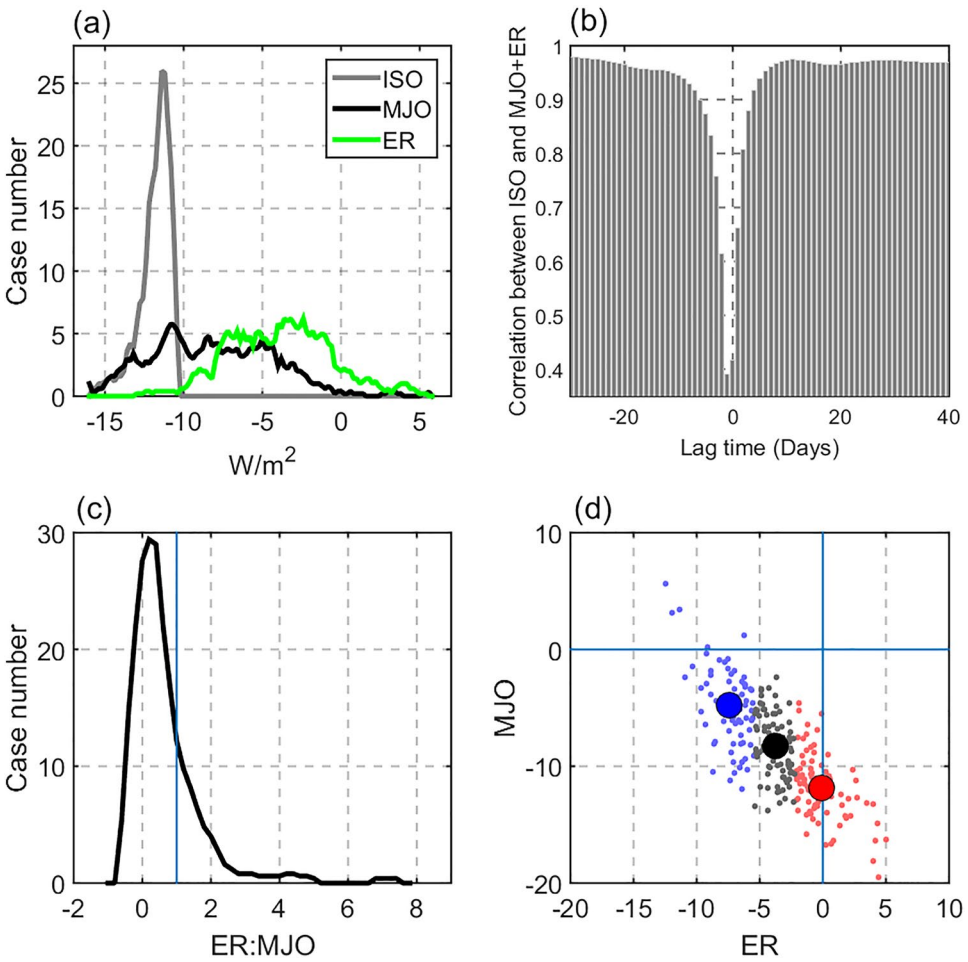

Fig. 1 **a** The histogram of OLR anomalies (W/m^2) averaged over the equatorial Indian Ocean (15° S–15° N, 70°–100° E) for (gray) ISO, (black) MJO and (green) ER wave on Day 0 of all ISO events. **b** The correlation coefficient in terms of anomalous OLR between ISO and MJO + ER on each lag day of selected ISO events. **c** The histogram of the ratio in OLR anomalies on Day 0 between ER and MJO. **d** The scatter diagram of ER versus MJO in terms of OLR anomalies on Day 0. Red, black and blue colors denote three scenarios of "Strong", "Moderate" and "Weak" ER, respectively. The ensemble mean in different scenarios is marked by large-size circles. See texts for definitions of Day 0 and three scenarios

mode (Fig. 2h, j), as the ER wave can propagate through both the northern and southern MC (Fig. 2i). Although the ER wave is weaker than the MJO, it still contributes to nearly one half the ISO strength in many regions, such as the Philippine Sea, the Southwest Indian Ocean, the Northwest Australia and the South Pacific (Fig. 2j). This implies that besides the canonical eastward propagation, we should also pay attention to westward-propagating signals in boreal winter to fully understand the ISO dynamics. For example, the ER wave over the Southwest Indian Ocean might help the ISO initiation (RF04b; Wei et al. 2019, 2023a); while over the Philippine Sea, it likely affects the ISO propagation diversity (Wei et al. 2023b).

Of particular interest is the land-sea contrast of the ISO strength over the MC (Sobel et al. 2008). We focus on a specific region of the MC, i.e., 7.5° S–10° N, 105°–150° E, and calculate the averaged STD over land and sea gird points (Table 1). A robust conclusion is that without the inference from the ER wave, the ratio between land and sea in the MJO increases to nearly 1.0. While in the total ISO, the land/sea ratio is much smaller (~0.75 in winter and ~0.80 in summer). The ratio for the ER wave (~0.90) is in between ISO and MJO. An intuitive explanation is that we have used spatial filtering to extract MJO and ER waves, which might smooth out the small-scale features in the MC. Nevertheless, the MJO + ER indeed does a good job in reproducing the island minimum, and the land/sea ratio even becomes smaller (Fig. 2g), as compared to the total ISO (Fig. 2f). Thus, we hypothesize that one may find another solution to the ISO minimum over the MC by examining MJO-ER wave interference effects, if any. We will revisit this issue in the following analysis.

Both the boreal summer and winter seasons are calculated.

Based on the ER/MJO ratio during boreal winter (Fig. 2j), we construct several indices by averaging the anomalous OLR of the ISO in four representative areas, including the Philippine Sea (7.5°–20° N, 125°–165° E), Northwest Australia (25°–15° S, 110°–130° E), Southwest Indian Ocean (15°–5° S, 40°–60° E) and South Pacific (15°–5° S, 160°–130° W). As we depicted above, the ER wave in these areas is equally, if not more, important than the MJO. Figure 3 shows the regressed zonal propagation of ISO, MJO and ER waves upon four ISO indices. Because our approach

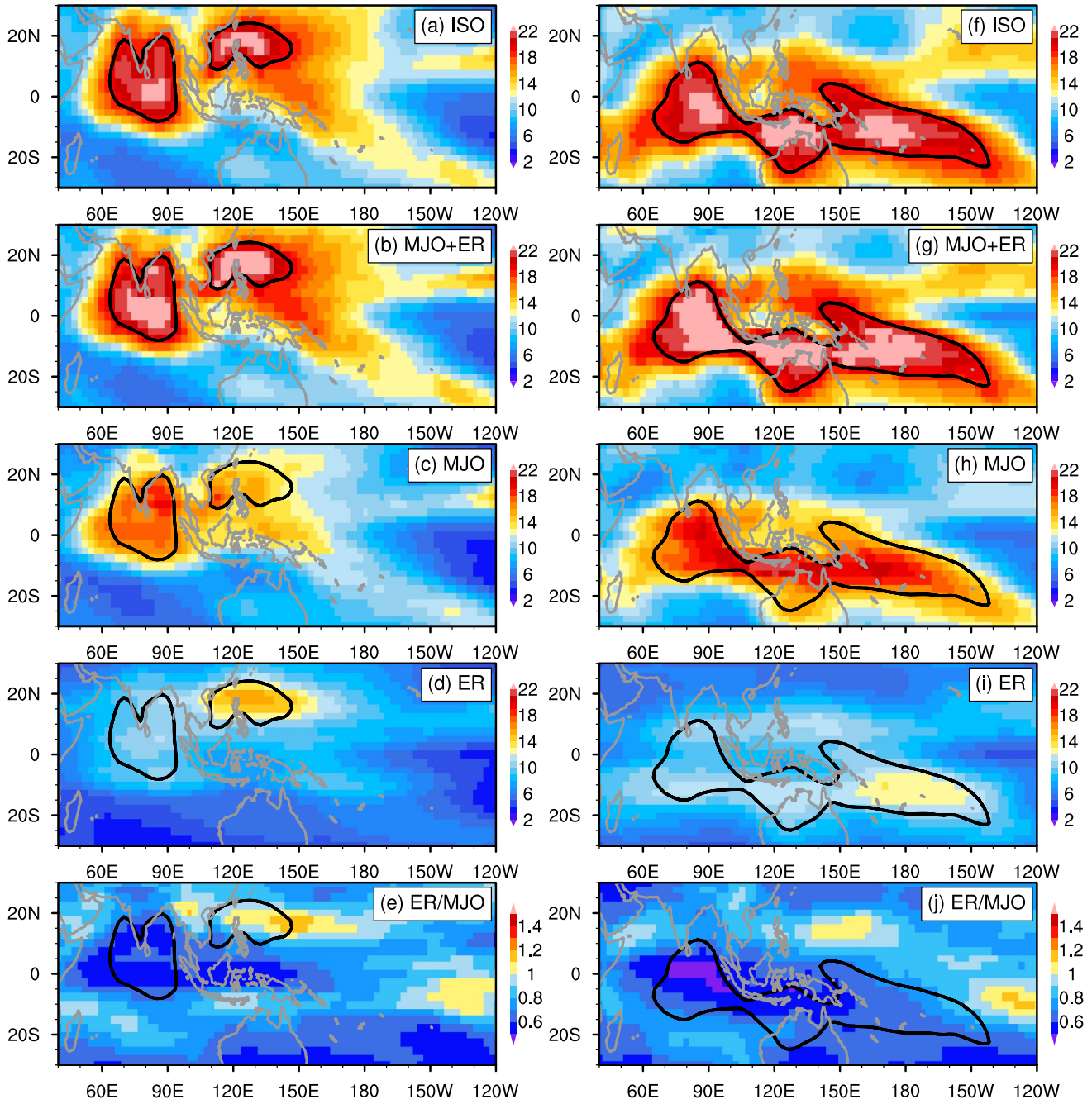

Fig. 2 The ISO strength and the relative contribution of MJO and ER wave modes. (Left) The STD of OLR anomalies (W/m^2) for **a** the ISO, **b** the sum of MJO and ER wave, **c** the MJO and **d** the ER wave during boreal summer. **e** The ratio in the STD between the ER wave and the MJO. The black contours in each panel denote the STD of 19.0 W/m^2 for the ISO. (Right) Same as the left panel, but for boreal winter

Table 1 The land-sea contrast in the strength of the ISO as well as its MJO and ER components over an area of the MC (7.5° S–10° N, 105°–150° E)

	Boreal summer (W/m^2)			Boreal winter (W/m^2)		
	ISO	MJO	ER	ISO	MJO	ER
Land	12.1	12.7	8.0	13.2	14.3	8.9
Sea	15.2	13.2	8.9	17.6	14.9	9.8
Land/Sea	0.79	0.96	0.90	0.74	0.96	0.91

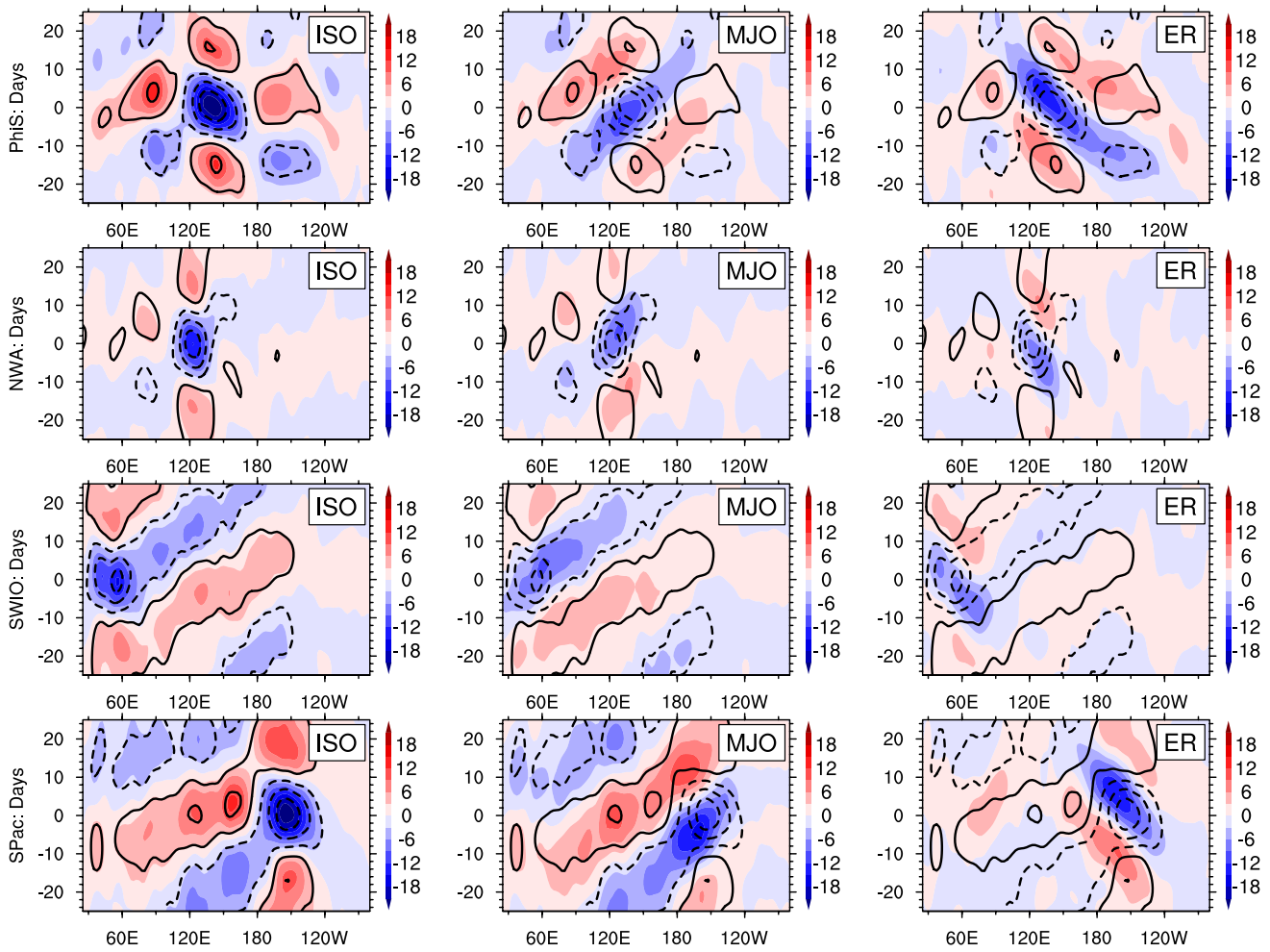

Fig. 3 Impacts of MJO-ER interferences on the ISO propagation during boreal winter. The shading shows the regressed ISO (Left), MJO (Middle) and ER wave (Right) upon the standardized ISO index, calculated as the OLR anomaly of the ISO over (**a**–**c**) the Philippine Sea (PhiS, 7.5°–20° N, 125°–165° E), **d**–**f** the Northwest Australia (NWA, 25°–15° S, 110°–130° E), **g**–**i** the Southwest Indian Ocean (SWIO, 15°–5° S, 40°–60° E), and (j-l) the South Pacific (SPac, 15°–5° S, 160°–130° W). Solid (dashed) contours in each panel denote the positive (negative) OLR anomalies for the ISO, with a contour interval of 3.0 W/m^2

includes all ER wave signals in the base index, it guarantees that a substantial amount of ER wave signal will appear in the regression results right at the base longitude. In contrast, the approach of RF04b finds the part of the ER wave signal best correlated with the eastward-filtered MJO index. That signal will not necessarily maximize at lag zero at the base longitude. Thus, our result will focus on ER waves that intersect constructively with the base index at lag = 0 days.

The intraseasonal convection manifests non-propagating-like ISOs in the first two rows of Fig. 3. When we decompose Day-0 deep convection into MJO and ER components, it could be traced back to convection initiation over the Indian Ocean and central-eastern Pacific, respectively. One may argue that Fourier methods artificially produce eastward and westward components with equal amplitude in where a "standing-like" ISO occurs (Zhang and Hendon 1997). Nevertheless, we do find many episodes, in which two convective centers of ISO (can be 60°–150° far away from each other) propagate in opposite directions and meet somewhere over the MC, causing localized strengthening of deep convection like a non-propagating ISO. Moreover, the two centers are well fit by MJO and ER wave modes, supporting the existence and importance of MJO-ER wave interference effects (see Fig. S2). In addition, due to the localized westward propagation of the ER wave, the ISO displays a sudden initiation over the Southwest Indian Ocean and an abrupt termination over the South Pacific (see bottom two rows of Fig. 3).

Previous studies have indicated a vigorous year-to-year variation of the ISO (Slingo et al. 1999; Liu et al. 2016; Wei and Ren 2019). Although the much stronger interannual variance occurs from December to June, the seasonality in

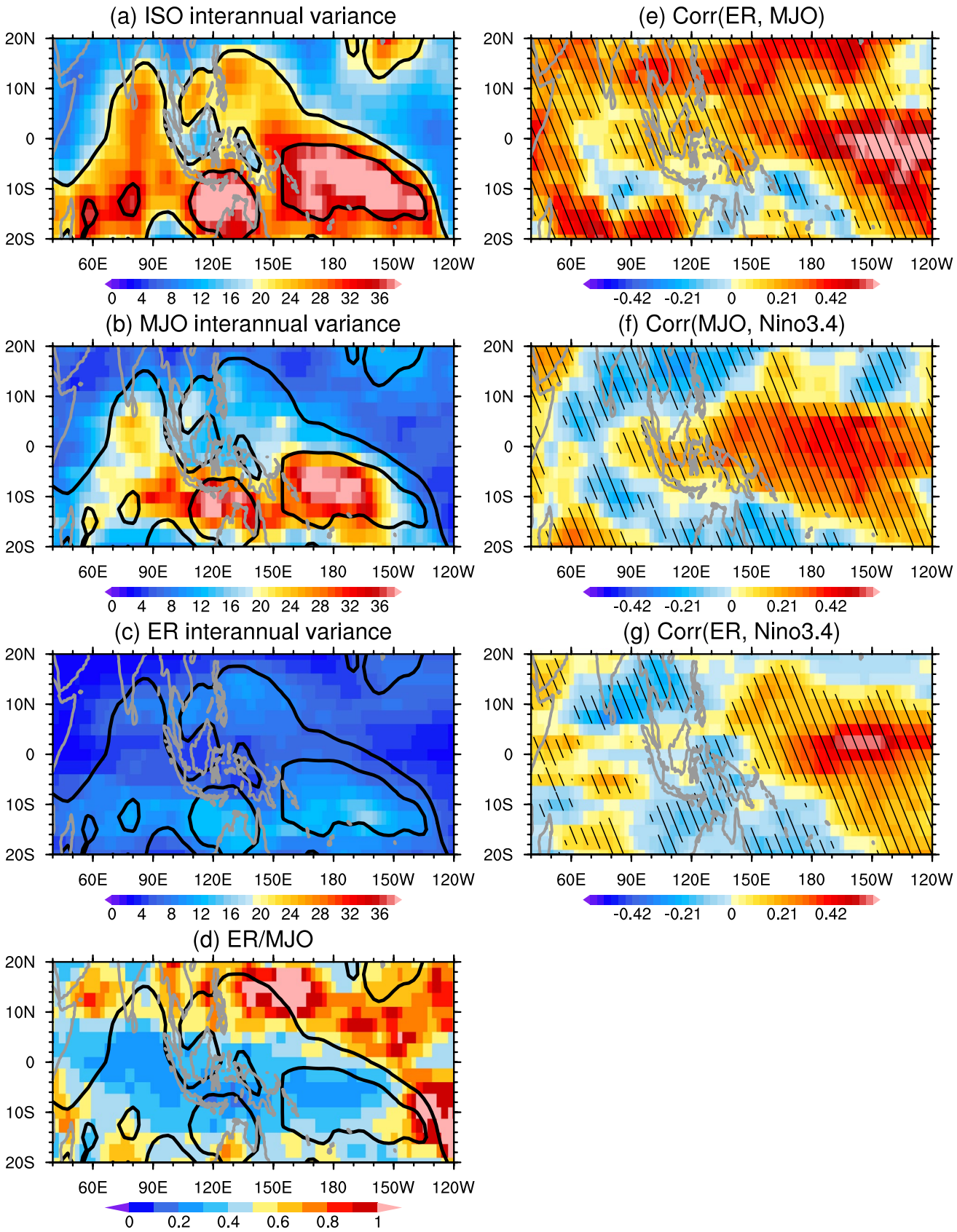
(a) ISO interannual variance
(b) MJO interannual variance
(c) ER interannual variance
(d) ER/MJO
(e) Corr(ER, MJO)
(f) Corr(MJO, Nino3.4)
(g) Corr(ER, Nino3.4)
20N
10N
0
10S
20S
60E
90E
120E
150E
180
150W
120W
0 4 8 12 16 20 24 28 32 36
0 0.2 0.4 0.6 0.8 1
-0.42 -0.21 0 0.21 0.42

◂**Fig. 4** The interannual variability of the ISO strength. The all-seasonal variance (W^2/m^4) of the monthly ISO strength with monthly climatology removed for **a** the ISO, **b** the MJO and **c** the ER wave. **d** The ratio map in the interannual variance between the ER wave and the MJO. The black contours in each panel show the interannual variance of 20.0 and 33.0 W^2/m^4. **e** The correlation coefficient in the monthly strength anomalies between the ER wave and the MJO. **f** The correlation coefficient between the Nino3.4 index and monthly MJO strength anomalies. **g** Same as (**f**), but for the ER wave. The hatched regions denote passing the Student t-test at the 90% confidence level

terms of the spatial distribution of the local maxima is small (figure not shown). Thus, we show here the all-seasonal pattern of the interannual variability of the ISO strength, which features two maximum centers over the southern MC and the South Pacific Convergence Zone (Fig. 4a). Although the MJO mode largely dominates inside of the ISO interannual variability (Fig. 4b), we cannot take no account of the contribution of ER wave, which is especially true near the northern and eastern edges of the ISO interannual variability (Fig. 4c, d). This suggests that the variation of the area of ISO activity on the interannual time scale could be largely regulated by ER waves besides the contribution of the MJO mode.

Do MJO and ER waves vary synchronously on the interannual time scale? We further calculate the correlation coefficient between MJO and ER wave in a monthly STD time series. As seen in Fig. 4e, MJO and ER waves show a positive correlation over most areas of the Indo-Pacific warm pool. Besides, the correlation is generally high outside of the main center of the ISO interannual variability, while it is lower inside and even turns negative in the southern MC. To understand this feature, we calculate the meridional gradient of monthly mean moisture (Q_y hereafter) over 14° S–4° S, 130° E–180° during boreal winter when the MJO detours via the southern MC. Interestingly, the correlation between the MJO strength and Q_y reaches 0.48, while it is only − 0.13 between the ER wave strength and Q_y. This reflects that the increase of Q_y tends to strengthen the MJO (Wei and Ren 2024) but possibly weaken the ER wave over the southern MC. Therefore, a weakly negative correlation between MJO and ER wave is observed. Over other regions, such as the central-eastern Pacific, the synchronous strengthening or weakening of MJO and ER waves may be related to the *in-situ* vertical wind shear (Wang and Xie 1996; Chen 2022b).

We further measure ENSO's impacts by calculating the correlation between the Niño3.4 index and the monthly STD time series of MJO (Fig. 4f) and ER wave (Fig. 4g). A significant positive correlation (~ 0.5) is observed over the western-central Pacific for both the MJO and ER waves, while over other regions, the correlation coefficient is generally small and its sign is strongly region-dependent. The correlation patterns derived here are similar to Huang and Huang (2011). The main difference in the correlation pattern between MJO and ER is observed over the central-southern MC. The correlation with the Niño3.4 is significantly positive for the MJO while negative for the ER mode. This contrast partly explains the even negative correlation over the southern MC seen in Fig. 4e. Based on Wei and Ren (2019), ENSO mainly affect the intraseasonal moistening or drying over the MC by modulating Q_y. When Q_y increases during El Niño, as we argue above, the MJO is strengthened while the ER activity decreases. Thus, inverse correlation patterns of MJO and ER shape over the MC. Also note that over the equatorial MC, although ENSO exerts inverse impacts on MJO and ER, the correlation between the two modes seen in Fig. 4e is weakly positive. This suggests that ENSO alone cannot explain all kinds of MJO-ER interannual variations. Future studies should examine ENSO-independent impacts on the ISO, MJO and ER from such as the Indian Ocean Basin Mode (Wang et al. 2024), Quasi-Biennial Oscillation (Martin et al. 2021), etc.

3.2 Impacts of MJO-ER interferences on the *ISO* structural organization

Distilling separate roles of MJO and ER wave might further our understanding of the structure of convective organization and its evolution in ISO's life cycle. During boreal summer, the regressed ISO based on the equatorial Indian Ocean (15° S–15° N, 70°–100° E) reference index shows a dipolar structure, with enhanced convection over the Indian Ocean and suppressed convection centered over the Philippine Sea (Fig. 5a). Additionally, as a typical feature of the boreal summer ISO (Kikuchi 2021), both the enhanced and suppressed convection tilt northwestward away from the equator. Interestingly, without the contamination of the ER wave, this northwest-southeast tilted structure becomes more evident for the "pure" MJO mode (Fig. 5b). In contrast, the ER wave itself displays a wave-train pattern and no clear tilt is observed (Fig. 5c). This suggests that the unique tilted structure of the boreal summer ISO, which many state-of-the-art climate models are struggling to capture (Neena et al. 2017), might root in the eastward-propagating MJO mode.

In boreal winter, the regressed ISO pattern highly resembles that commonly documented in many studies (e.g., Wheeler and Hendon 2004; Matthews 2008; Kiladis et al. 2014), featuring enhanced convection over the Indian Ocean and suppressed convection over the western Pacific (Fig. 5d). What we would like to highlight here are the two suppressed convection centers over respectively the Philippine Sea and the South Pacific Convergence Zone, which are virtually sourced distinctively. Though the latter is determined by the MJO (Fig. 5e), the former results from the combination of MJO and ER modes (Fig. 5f). Besides, the two centers are further separated by the moist ER wave signal over the equatorial western Pacific. In other words, without impacts of the ER wave, one cannot obtain two convective centers

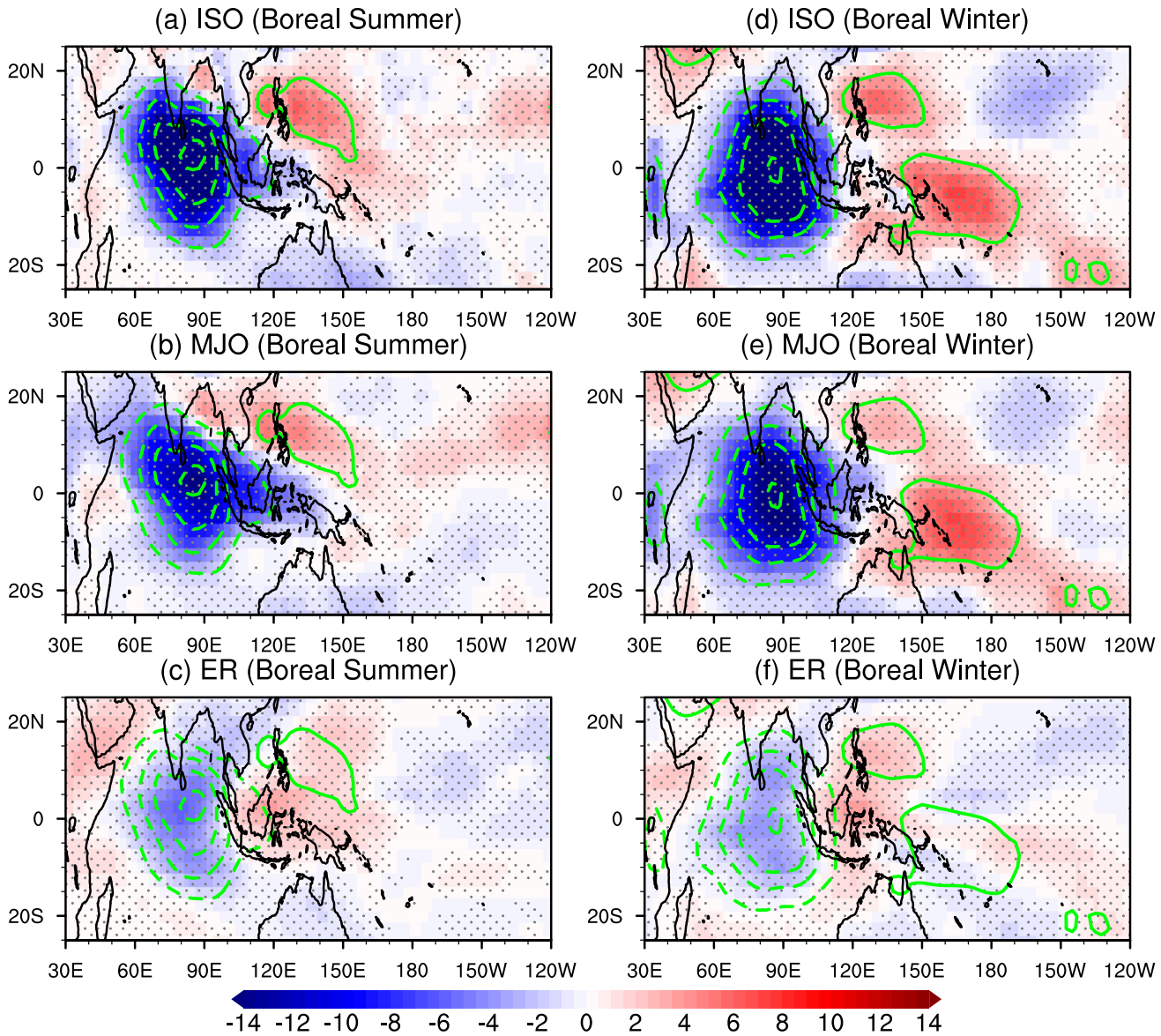

Fig. 5 The regressed ISO structure. (Left) Regressed OLR anomalies (W/m^2) for **a** the ISO, **b** the MJO and **c** the ER wave upon the ISO index over the Indian Ocean (15° S–15° N, 70°–100° E) during boreal summer. Solid (dashed) green contours in each panel show positive (negative) OLR anomalies of the ISO, with a contour interval of 3.0 W/m^2. The zero contours are omitted. The stipple denotes passing the Student-t test at the 90% confidence level. (Right) Same as the left panel, but for boreal winter

straddling the equator. It is also interesting to assess how many climate models can reproduce these ER wave-induced features of the boreal winter ISO in future studies.

To understand the northwest-southeast tilted structure of the MJO mode during boreal summer (Fig. 5b), we compare the MJO propagation near the equator (5° S–5° N, Fig. 6a) and that 15° off the equator (10°–20° N, Fig. 6b). Previous studies mostly emphasized the northward propagation (e.g., Wang and Xie 1997; Karmakar and Misra 2020; Konda and Vissa 2022), while here we propose a new interpretation based on the eastward propagation. When the equatorial convection reaches such as the MC (Fig. 6b), the off-equatorial convection just arrives at the Indian Ocean (Fig. 6a), implying a fast speed near the equator. By referring to green arrows in Fig. 6, we calculated a fast speed of 26° longitude/phase in 5° S–5° N and a slow speed of 16° longitude/phase in 10°–20° N. Why are MJO speeds distinct in different latitude bands? By comparing composite 850-hPa zonal wind anomalies, we find that the equatorial Kelvin-wave easterly wind anomaly to the east of 150° E is two times stronger than the off-equatorial easterly (Fig. S3a–b), thus supporting a fast propagation speed (Wang et al. 2019). Besides, a faster equatorial propagation is also associated with a stronger zonal asymmetry of the column-integrated

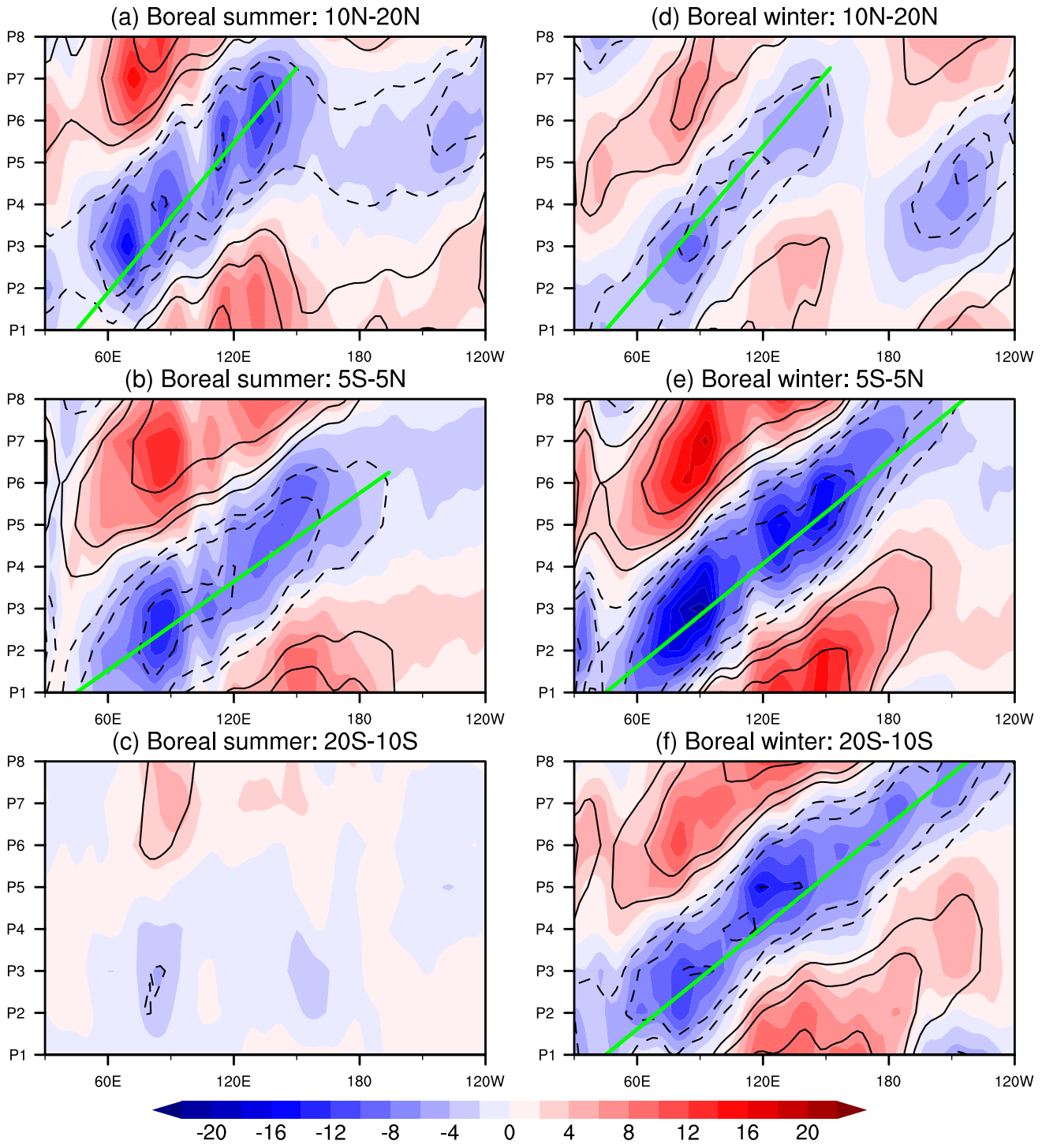

Fig. 6 The latitudinal dependence of the eastward phase speed of the MJO mode. (Left) Composite OLR anomalies over 10° N–20° N, 5° S–5° N, and 20° S–10° S in each RMM phase for the ISO (shading) and the MJO (black contour) during boreal summer. Solid (dashed) contours denote positive (negative) anomalies, with a contour interval of 3.0 W/m^2. The zero contours are omitted. The green arrow denotes the phase speed line. (Right) Same as the left panel, but for boreal winter

moisture tendency (Figs. S4a–b). These dynamical wave and moisture-convection feedbacks have been used to understand mechanisms of MJO propagation and ENSO modulations on fast and slow MJO modes (Hsu and Li 2012; Chen and Wang 2018; Wei and Ren 2019; Wei et al. 2022). However, the aforementioned contrasts are not seen for the MJO during

boreal winter (Figs. S3c–d and S4c–d), which explain similar propagation speeds (~22° longitude/phase) of convection in 5° S–5° N (Fig. 6e) and 20° S–10° S (Fig. 6f).

Figure 5 only informs the roles of MJO and ER wave in one phase of the ISO. Then, what are their relative contributions to the ISO in different phases? Here, we show ratio maps of composite OLR anomalies between ER and MJO in eight RMM phases. Only those days with the RMM amplitude exceeding one are included. The positive ratio denotes a constructive interference effect between ER and MJO, while a negative ratio implies a destructive effect on the ISO. To observe spatiotemporal evolutions of ISO, we also overlay ± 3 W/m^2 OLR anomalies as references. Note that the convective anomaly of the MJO mode always keeps the same sign as the ISO and thus MJO-ER interference effects mainly arise from the ER mode. Our results indicate that the ratio map in Phases 1–4 is similar to Phases 5–8, though a dry–wet asymmetry could be detected. During boreal summer, for example, the contribution of the ER mode to the wet ISO convection over the Philippine Sea in Phase 7 is considerably larger than that to the dry convection in Phase 3 (Fig. 7). However, this Phase 3–7 asymmetry reverses during boreal winter, featuring a larger ER contribution to the dry ISO convection in Phase 3 (Fig. 8). Additionally, the interference effect is region-dependent and is generally strong along the edge of ISO envelopes, which is consistent with Fig. 4d. What is even more interesting is the strengthened negative ratio along the east edge of ISO envelope that is heading east across the MC (e.g., Phases 3 and 7). This lends us to conjecture that the dry convection of ER waves might propagate into the MC and reduce the intensity of the moist envelope of ISO. In other words, the ER wave is hypothesized here to be among the reasons for MC damping effects on the ISO.

Here we find evidences to support the above conjecture by observing individual ISO events, in which independent

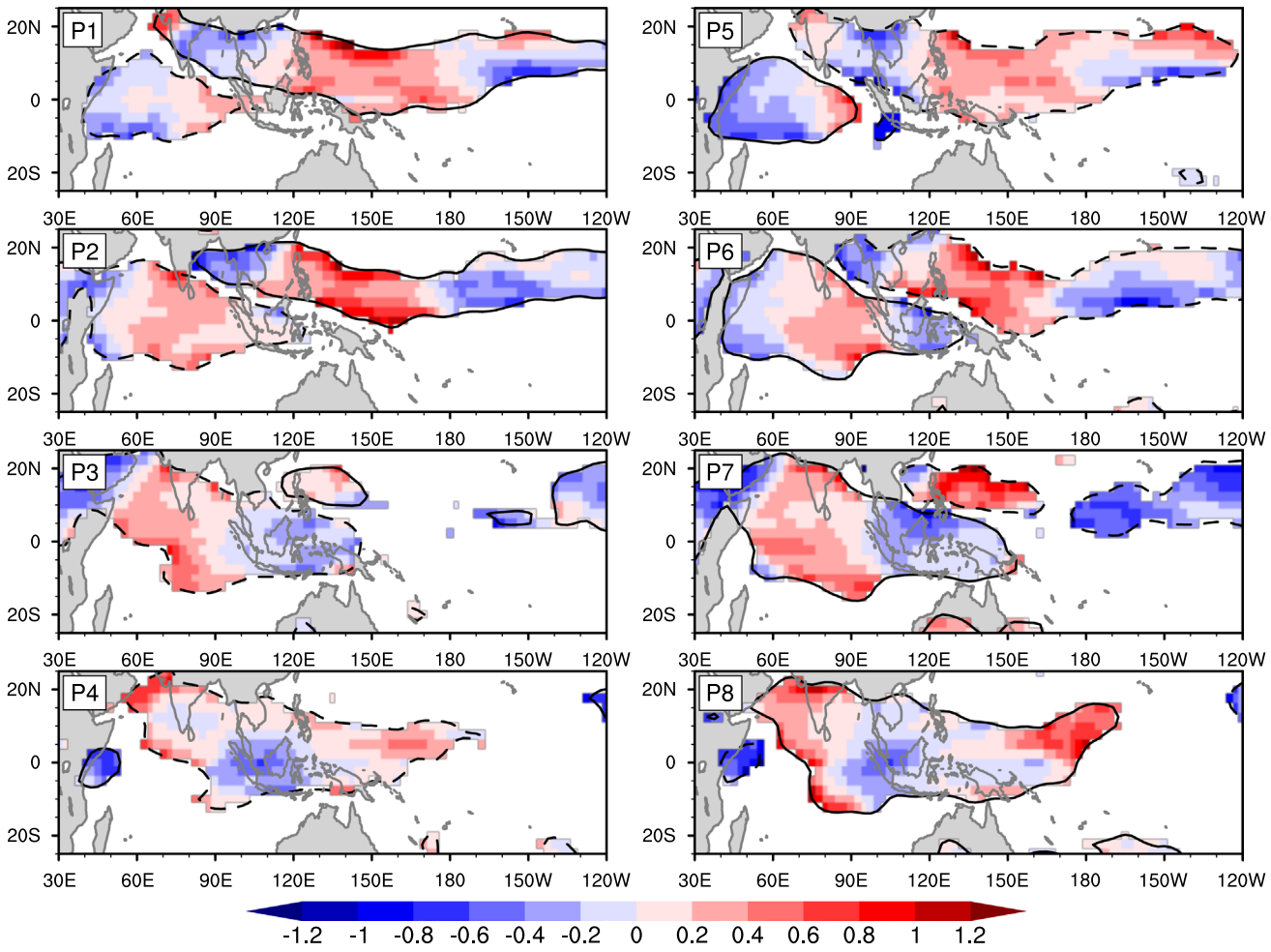

Fig. 7 Relative contributions of MJO and ER to the ISO in eight RMM phases. Shown are the ratio maps of composite OLR anomalies between ER and MJO during boreal summer. The red color denotes that ER and MJO are in opposite sign, while the blue color indicates the same sign shared by the two. The solid (dashed) black contour shows OLR anomalies of ISO exceeding 3 (-3) W/m^2 that pass the Student *t* test at the 95% confidence level

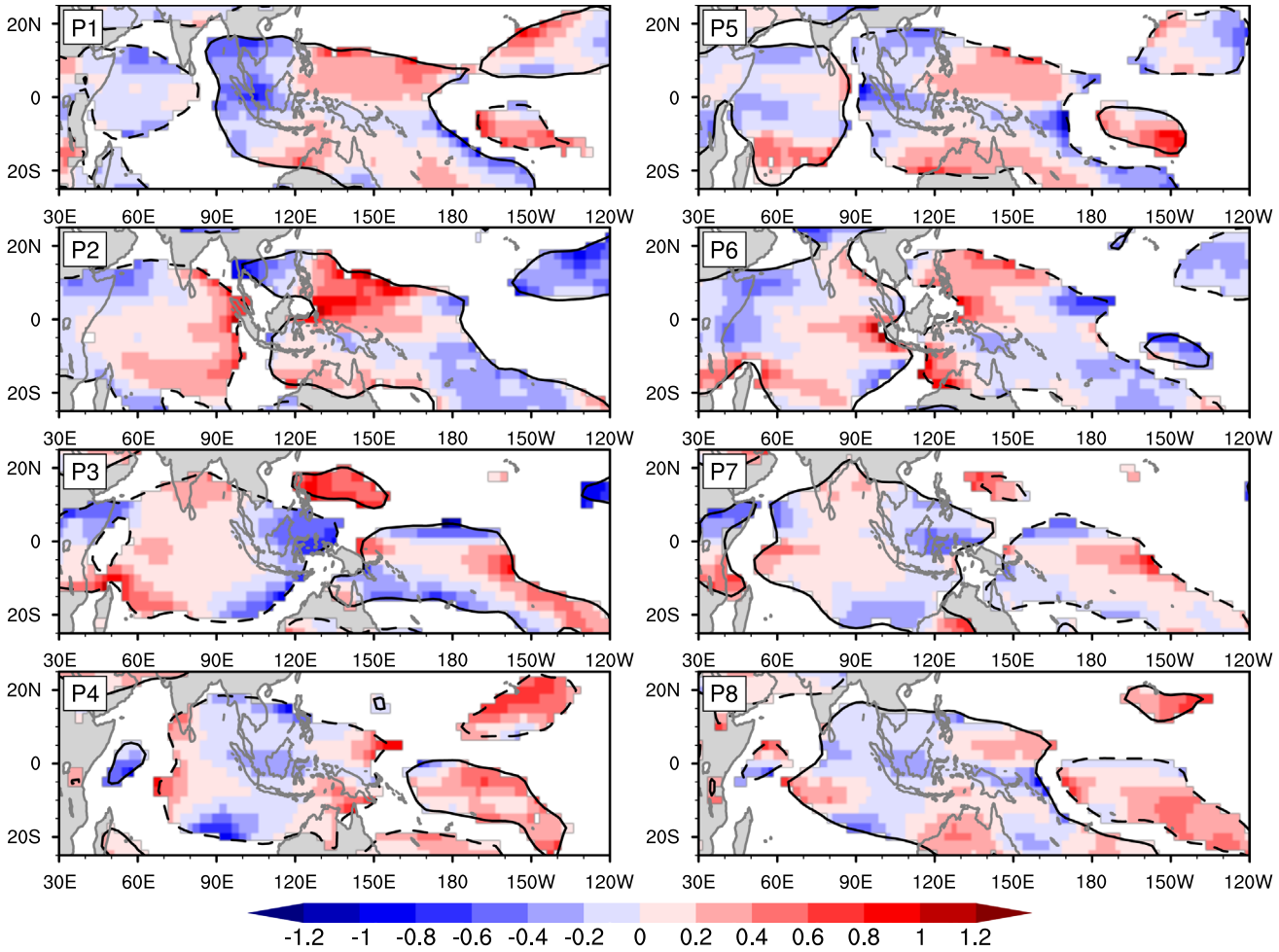

Fig. 8 Same as Fig. 7, but for the boreal winter

ER wave and MJO are propagating in opposite directions and cause destructive effects on the deep convection of ISO over the MC. Several cases of such ISO events and their composite are shown in Fig. 9. As seen in Fig. 9f, the total ISO decays considerably over the MC, before which there exists a westward-propagating dry ISO signal initiated from the far central-eastern Pacific. This dry ISO signal is dominated by the westward-propagating ER wave mode. Without the dry intrusion of the ER wave, the MJO itself is only weakly damped (may be due to land friction, diurnal cycle, etc.) over the MC. How is the preceding ER wave triggered? One answer is the MC damping itself, which naturally generates westward-propagating waves like ER waves (Zhang and Hendon 1997). However, this may not be true here, as the ER wave signals emerge in the hövmoller diagram distantly from the intersection points and at several days of time lag. One may find the other eastward-propagating deep convection of ISO before Day 0, which decays quickly upon approaching cold waters in the central-eastern Pacific. The aftermath is the decoupling of the Rossby wave component from the ISO on approximately Day − 25, which is similar to the paradigm proposed in previous studies (e.g., Wang and Xie 1997; Komaromi et al. 2019). Under some circumstances (e.g., La Niña), an exceptionally strong ER wave could even cause a non-propagating ISO (Feng et al. 2015; DeMott et al. 2018; Wei et al. 2023b).

An intuition is that background conditions that favor the breakdown of an MJO event over the MC might also simultaneously discourage the ER wave propagation. However, this may not necessarily hold. For example, during La Niña winters, the meridional distribution of the background mean moisture over the MC becomes less steep (and thus Q_y is decreased) due to a wetter than normal environment off the equator (see Fig. 8 in Wei and Ren 2019). Consequently, it is difficult for the MJO to cross through the southern MC, as the eastward-propagating mechanism dominated by the Q_y-related meridional moisture advection (Kim et al. 2017) becomes inefficient. However, as we have argued above, the ER wave over the southern MC might become stronger with a decreased Q_y during La Niña (see also Fig. 4g). Thus, the

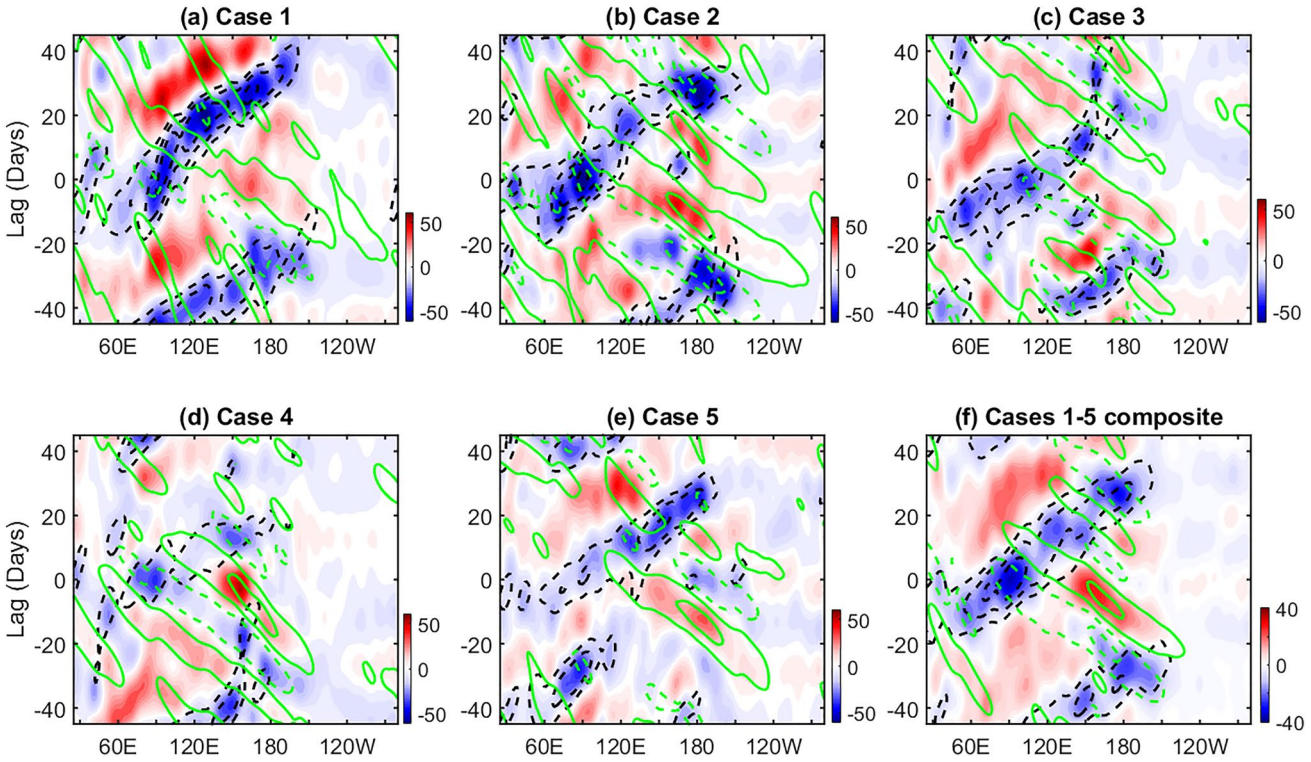

Fig. 9 Time-longitude sections of OLR anomalies (W/m^2, 7.5° N–20° N averaged) for the ISO (shading), the MJO mode (black dashed contour) and the ER wave mode (green solid contour) for **a**–**e** five selected cases and **f** their composite pattern. These cases were selected based on OLR anomalies of the ISO averaged over 10° S–10° N, 70°–100° E lower than one negative standard deviation. "Lag 0" denotes the day when the deep convection of the ISO reaches the local maximum over the Indian Ocean. Solid (dashed) contours denote positive (negative) anomalies and start from ± 5 W/m^2, with an interval of 15 W/m^2 for panels (**a**–**e**) and 10 W/ m^2 for panel (**f**). Note that different color ranges are used in different panels

ER wave activity could correlate with the La Niña conditions known to discourage MJO propagation through the MC (Wei and Ren 2019; Wang et al. 2019).

These results give us implications for comprehending issues of current climate models in exaggerating the "MC barrier effect". Most climate models simulate a stronger ER wave (or equivalent to a smaller East/West ratio of intraseasonal timescale power variance) as compared to observations (Kim et al. 2009; Jiang et al. 2015; Ahn et al. 2017), which might exert a major damping effect on the ISO when crossing the MC islands. This issue calls for in-depth studies in the future.

3.3 Impacts of ER waves on the *ISO* Initiation

Motivated by recent studies (Feng and Li 2016; Wei et al. 2019, 2023a, b), we investigate the impacts of ER waves on the ISO initiation from the Indian Ocean. Figures 10a–c show the OMI evolution of selected ISO events from Day − 25 to Day 20, and Fig. 10d–f are histograms of OMI Phases 1–8 and No-ISO case (i.e., the OMI amplitude < 1) on Days − 5 and 0 under Weak, Moderate and Strong ER scenarios. See "Methods" for definitions of "Day 0" and three scenarios. As expected from the ISO selection method, OMI is generally manifested as Phases 2 and 3 on Day 0 regardless of the initial strength of the ER wave in different scenarios, implying that most events have developed into a zonal dipole with enhanced convection over the Indian Ocean and suppressed convection over the western Pacific. However, the ISO is preceded distinctively depending on the strength of the initial ER wave. For example, the OMI is mostly in Phases 1–2 five days ahead of Day 0 when the initial ER wave is weak. The OMI status of Day − 5 changes sharply with the increase of the initial ER wave strength. Under the Strong ER scenario, most ISOs start dramatically from the No-ISO status. Thus, we conjecture that the "primary" type of ISO events (Matthews 2008) likely become more favorable with the strengthening of the initial ER wave. To confirm our hypothesis, we select "successive" events when the OMI amplitude exceeds a prescribed threshold (labeled α) in consecutive days (β) before Day 0. The remaining cases are the primary events. Seen from Fig. 10g–i, the ratio of primary events indeed increases robustly from Weak to Strong ER scenarios.

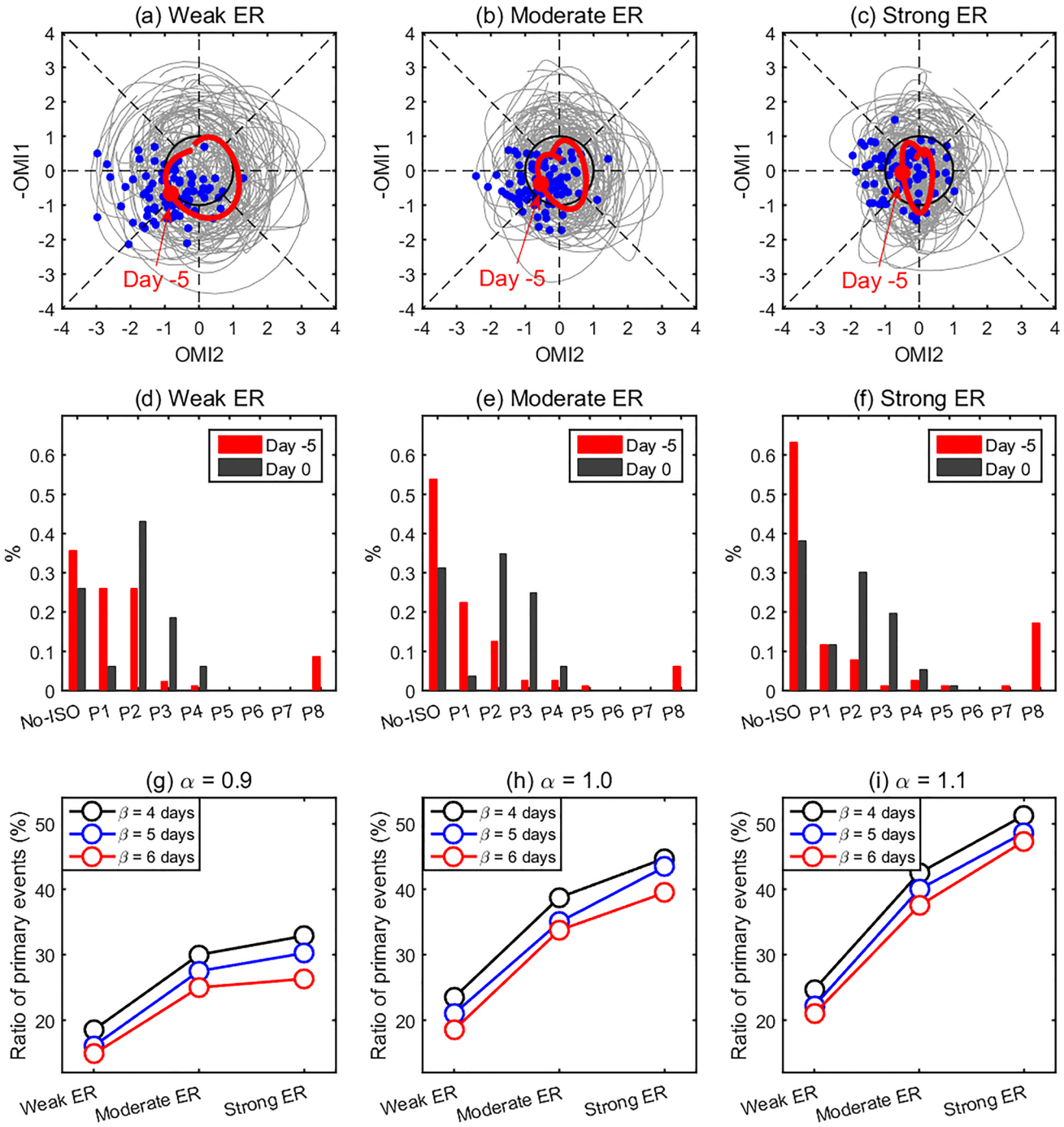

Fig. 10 The features of the ISO initiation conditioned by the strength of the ER wave over the Indian Ocean. **a** The OMI trajectory of selected ISO events from Days − 20 to 25 under the Weak ER scenario. Gray lines indicate individual ISO cases (Day − 5 as blue dots), while the red line is the all-case composite (Day − 5 as a red dot). **b**, **c** Same as (**a**), but for the Moderate and Strong ER scenarios, respectively. See Methods for the definition of Day 0 and three scenarios. (d) The histogram analysis (in %) of the OMI status for all ISO events on Day − 5 (the red bar) and Day 0 (the black bar) under the Weak ER scenario. **e**, **f** are the same as (**d**), but for the Moderate and Strong ER scenarios, respectively. **g**, **h** The ratio of primary events as a function of the ER wave strength over the Indian Ocean at the initiation of the ISO. The parameter α denotes the OMI amplitude threshold and β indicates the length of time (before Day 0) during which the OMI amplitude must remain above α for defining successive events

It is of equal importance to examine the subsequent ISO evolution after Day 0 if we include the "propagation" as a key ingredient for defining the ISO initiation (Straub 2013). As seen from Fig. 10a–c, the OMI amplitude in Phases 8–1 and 4–5 becomes smaller when the initial ER wave is stronger. This implies that the propagation of ISO convection might be weakened considerably over the MC with the strengthening of the initial ER wave over the Indian Ocean. Figure 11 offers the lagged composite of OLR anomalies (10° S–10° N averaged) for the ISO and ER wave under three scenarios, with their horizontal maps shown in Figs. S5–6. When the initial ER is weak, the propagation pattern of ISO displays an analog of successive events (Matthews 2008), featuring a circumnavigating mode immediately preceding the deep convection initiated on Day 0 (Fig. 11a). In contrast, when the initial ER becomes strong, no significant convection propagation is observed over the Western Hemisphere, and the Day-0 convection is probably initiated by a local suppressed convection over the eastern Indian Ocean (Fig. 11c), as is typical for primary events. Moreover, due to the considerable damping of deep convection over the MC, the ISO displays a "jumping-like" propagation behavior (Wang et al. 2019), thus reflecting a novel initiation-propagation linkage for the ISO (Wei et al. 2023a). The propagation pattern of ISO under the Moderate ER scenario is in between Weak and Strong ER scenarios, showing a primary-successive mixture event (Fig. 11b).

Also seen from hovmöller diagrams in Fig. 11c, a moist signal of ER waves is triggered from the western Pacific and is associated with enhanced deep convection over the central Pacific on about Day − 20. The ER wave propagates westward into the Indian Ocean and helps initiate the ISO deep convection on Day 0. This paradigm is quite similar to the new initiation mechanism of primary events documented recently (Wei et al. 2019, 2023a). Thus, we might monitor and/or predict the ISO onset early by identifying the precursor signals of ER waves.

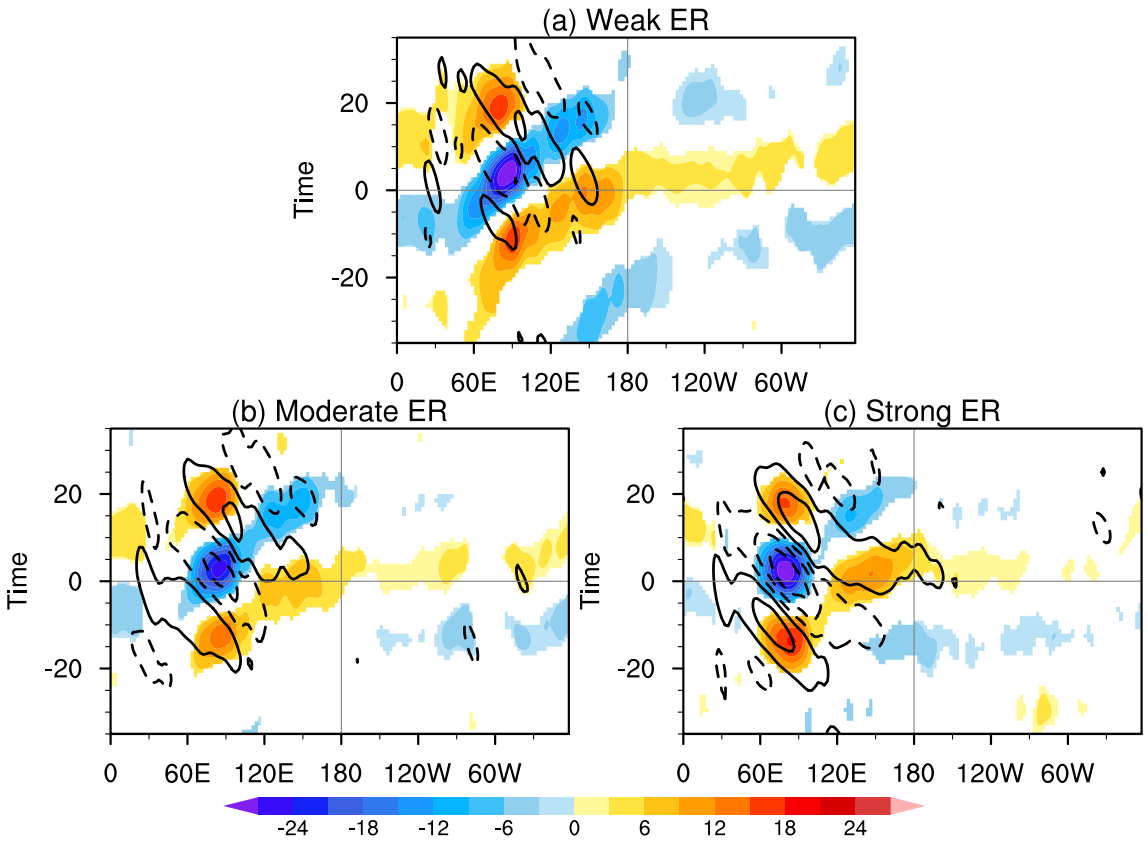

Fig. 11 The dependence of ISO initiation on the preceding ER wave strength over the Indian Ocean. **a** Lagged composite of 10S–10N averaged OLR anomalies (W/m^2) of ISO (shading) and ER wave (black contours) for ISO events under the Weak ER scenario. Solid (dashed) contours denote positive (negative) anomalies, starting from ± 2 W/m^2 and with a contour interval of 5.0 W/m^2. Only those passing the Student *t* test at the 95% confidence level are shaded. **b**, **c** Same as (**a**), but for the Moderate and Strong ER scenarios, respectively

4 Conclusion and discussion

4.1 Concluding remarks

Recent studies have detected potential roles of ER wave signals in the initiation and propagation of the ISO (Wei et al. 2019, 2023a, b). We were so motivated that isolating ER and MJO components from the total ISO might shed new light on the fundamentals of the ISO. Although this topic is not new (RF04b), some major issues remain elusive and are thus investigated in this study.

Distinct contributions of MJO and ER modes to the ISO strength have been quantified, with seasonality and regionality emphasized. During boreal summer, the Northwest Pacific ISO mainly owes its existence to the ER mode, while over the Indian Ocean, the MJO mode is dominant. During boreal winter, despite the major contribution of the MJO mode, over where the ER wave is sufficiently strong, the ISO shows non-canonical behaviors of non-propagating convection and sudden initiation and termination. These generally arise from constructive or destructive interferences of MJO and ER modes, which cause localized strengthening or weakening of convective anomalies.

For the ISO interannual variability, the strength inside is mainly controlled by the MJO. Along the edge, however, the ER's contribution becomes comparable to the MJO and even dominant along the eastern edge. This suggests that the variation of the area of ISO activity on the interannual time scale is largely regulated by the ER mode. MJO and ER modes vary synchronously on the interannual time scale over the western-central Pacific, where ENSO serves as an important modulating factor. The warm ENSO phase supports the strengthening of both MJO and ER modes; however, in the cold ENSO phase, both components are weakened over the western-central Pacific. Over the MC, the MJO is positively correlated with ENSO, while ER is negatively correlated. These inverse ENSO impacts on MJO and ER modes are associated with the meridional gradient of mean moisture over the MC. During La Niña, for example, the reduced moisture gradient over the MC weakens the MJO but likely promote the ER activity.

MJO and ER modes play distinct roles in shaping the ISO structure in different seasons. For example, the northwest-southeast tilted convection of the boreal summer ISO is rooted in the MJO mode, which features a decreasing phase speed away from the equator. During boreal winter, when ISO deep convection peaks over the Indian Ocean, the ER mode helps shape two leading suppressed convection centers over the South Pacific Convergence Zone and the Philippine Sea. We further reveal that the MJO-ER interference is rooted in the ER mode and most significant along the edge of ISO envelopes. Moreover, the ER's contribution to the ISO depends on the ISO phases and seasons. For example, it is strong over the Philippine Sea in the ISO wet phase (i.e., Phase 7) during boreal summer, while it becomes weak during boreal winter. The opposite, however, holds in the ISO dry phase (i.e., Phase 3).

Additionally, the MJO-ER interference can be used to explain the damping effect of MC on the ISO. Unlike the total ISO, the MJO itself does not decay considerably over the MC. However, a westward-propagating dry signal of the ER wave, which can be detected early over the central-eastern Pacific, can intrude the MC and cause a further decaying of the MJO deep convection. Zhang and Hendon (1997) suggested that the damped ISO could naturally generate westward-propagating waves like the ER mode. But here, we have identified episodes in which an eastward MJO and a westward ER are initially far away from each other, then meet somewhere over the MC and finally cause considerably weakened ISO convection. We argue that the background conditions that favor breakdown of MJO may not simultaneously discourage the ER wave propagation. For example, although likely blocking the MJO by flatting longitudinally the MC ambient moisture, the La Niña could strengthen the ER wave activity over the MC.

Finally, we find that the initiation of the ISO deep convection over the Indian Ocean is related to the strength of the preceding ER wave signal. More specifically, a primary event is probably expected when observing strong moist ER wave signals over the Indian Ocean. Otherwise, the occurrence likelihood of a successive ISO event increases. Additionally, the ER wave-regulated initiation manner of the ISO can predict the subsequent propagation pattern of ISO. For example, a "jumping-like" ISO is more favorable when the Indian Ocean is preconditioned by a strong ER wave, implying an "initiation-propagation linkage" of the ISO (Wei et al. 2023a).

4.2 Discussion

The ER wave is usually emphasized for the boreal summer ISO but not for the boreal winter ISO. This study suggests that the ER wave is also worthy of investigation during boreal winter. Two important features highlighted here are the ISO minimum over the MC and the ISO initiation from the Indian Ocean, which are unraveled here due partly to the impacts of the ER wave. Most state-of-the-art climate models are still struggling to capture these two ISO features (Jiang et al. 2015; Neena et al. 2017; Ahn et al. 2017), which is possibly attributed to the overestimated or underestimated ER wave variability (Kim et al. 2009). Perhaps in the next step of work, one should include westward-propagating ER waves in a theoretical ISO model to simulate the episodic ISO initiation and the MC "barrier effect". A realistic simulation of the ER wave in subseasonal forecasting models

might improve the prediction of the ISO (Komaromi et al. 2019) and thus its far-reaching impacts.

Note that the ER waves examined here (subjected to the 20–100-day bandpass filtering) are more related to the low-frequency westward-propagating modes, while previous studies usually extracted the ER wave as a high-frequency (e.g., 10–30-day) mode (e.g., Yang et al. 2007a, 2007b; Feng et al. 2015; DeMott et al. 2018). The low-frequency ER wave might distinguish essentially from the high-frequency ER wave. On the basis of Fig. 4g, for example, we show that the low-frequency ER wave over the central-eastern Pacific has a significant positive correlation with the ENSO, which is consistent with Huang and Huang (2011) who also explored the interannual variability of ER waves with low-frequency components included. However, in several other studies investigating the interannual variability of high-frequency ER waves, the ENSO's impacts were weak and even negatively correlated with the ER wave (e.g., Wang and Chen 2016; Yang et al. 2016). It's not clear what the cut-off frequency is that distinguishes low- and high-frequency ER waves in terms of the ENSO's impacts. Why does the ENSO-ER wave correlation depend on the frequency of the ER wave? These important issues should be addressed in future studies.

Our results represented here might prompt a better understanding of the ISO and thus serve as benchmarks for evaluating contemporary climate models in simulating some salient features the ISO, such as its horizontal structure and complex propagation patterns. Based on our results, an alternative idea to attribute the model biases could be the assessment of the low-frequency (i.e., 20–100-day) ER wave and its interference effects with the MJO mode. We highlight that a reasonable simulation of the low-frequency ER wave should improve the representation skill of overall characteristics of the ISO in operational subseasonal models, thereby improving forecasting skills of extreme weather and climate events in a global warming background.

Some caveats are finally stated here. The regression and composite analysis methods used in this study have virtually averaged all ISO events. However, the emergence of an anomaly in a lagged regression diagram does not necessarily relate well with where the signals actually tend to originate. The problem is that events vary in phase speed relative to each other, so that events included in the analysis come out of phase with each other at long distances or at long time lags, effectively averaging each other out. The signals emerge not necessarily where and when new events occur, but instead where their historical phasing substantially agrees with the signals of other events centered at the base point. If the signal is statistically significant at a given time lag and longitude, it does show that signal tends to be present at that point relative to a signal at lag zero and the base point, but it does not necessarily show that the signal originated at the point where it becomes significant. Classifying fast and slow ISO events (Wei and Ren 2019) may be an alternative way to address this issue, which is left for future studies.

Supplementary Information The online version contains supplementary material available at https://doi.org/10.1007/s00382-024-07380-2.

Acknowledgements We would like to acknowledge two anonymous reviewers that help improve the representation of the paper. This study is jointly supported by the National Natural Science Foundation of China (Grant No. 42305056 and U2242206) and the Special operating fundings of scientific research institutions for "Key Technology Development of Numerical Forecasting" and the Basic Research and Operational Special Projects (2023Z024 and 2023Z003) of Chinese Academy of Meteorological Sciences. Y. Wei thanks the funding support of LASG.

Data availability The OLR data was from the NOAA/OAR/ESRL PSD, Boulder, Colorado, available at https://psl.noaa.gov/thredds/catalog/Datasets/interp_OLR/catalog.html. The ERA5 reanalysis data was available at https://doi.org/https://doi.org/10.24381/cds.bd0915c6. The NOAA ERSSTv5 was available at https://psl.noaa.gov/data/gridded/data.noaa.ersst.v5.html.

Declarations

Conflict of interest The authors do not have any relevant financial or non-financial interests to disclose.

References

Adames ÁF, Kim D (2016) The MJO as a dispersive, convectively coupled moisture wave: theory and observations. J Atmos Sci 73(3):913–941

Adames ÁF, Maloney ED (2020) Moisture mode theory's contribution to advances in our understanding of the Madden-Julian oscillation and other tropical disturbances. Curr Clim Change Reports 7:72–85

Adames ÁF, Kim D, Clark SK, Ming Y, Inoue K (2019) Scale analysis of moist thermodynamics in a simple model and the relationship between moisture modes and gravity waves. J Atmos Sci 76(12):3863–3881

Ahmed F (2021) The MJO on the equatorial beta plane: an eastward-propagating Rossby wave induced by meridional moisture advection. J Atmos Sci 78:3115–3135

Ahn M et al (2017) MJO simulation in CMIP5 climate models: MJO skill metrics and process-oriented diagnosis. Clim Dyn 49:4023–4045

Ahn M et al (2020) MJO propagation across the Maritime Continent: are CMIP6 models better than CMIP5 models? Geophys Res Lett. https://doi.org/10.1029/2020gl087250

Chen G, Wang B (2018) Effects of enhanced front Walker cell on the eastward propagation of the MJO. J Clim 31(19):7719–7738

Chen G (2022a) The amplification of Madden–Julian oscillation boosted by temperature feedback. J Atmos Sci 79(1):51–72

Chen G (2022b) A model of the convectively coupled equatorial Rossby wave over the indo-pacific warm pool. J Atmos Sci 79(9):2267–2283

Chen G et al (2022) The MJO from CMIP5 to CMIP6: perspectives from tracking MJO precipitation. Geophys Res Lett 49(1):e2021GL095241. https://doi.org/10.1029/2021gl095241

DeMott CA, Wolding BO, Maloney ED, Randall DA (2018) Atmospheric mechanisms for MJO decay over the Maritime Continent. J Geophys Res Atmos 123(10):5188–5204
Duchon CE (1979) Lanczos filtering in one and two dimensions. J Appl Meteor 18:1016–1022
Emanuel KA (1987) An air-sea interaction model of intraseasonal oscillations in the tropics. J Atmos Sci 44(16):2324–2340
Feng J, Li T (2016) Initiation mechanisms for a successive MJO event and a primary MJO event during boreal winter of 2000–2001. J Trop Meteorol. https://doi.org/10.16555/j.1006-8775.2016.04.004
Feng J, Li T, Zhu W (2015) Propagating and nonpropagating MJO events over Maritime Continent. J Clim 28(21):8430–8449
Fuchs Ž, Raymond DJ (2017) A simple model of intraseasonal oscillations. J Adv Mod Earth Sys 9:1195–1211
Fuchs Ž, Raymond DJ, Senti S (2019) A simple model of convectively coupled equatorial Rossby waves. J Adv Mod Earth Syst 11(1):173–184
Gloeckler LC, Roundy PE (2013) Modulation of the extratropical circulation by combined activity of the Madden–Julian Oscillation and equatorial Rossby waves during boreal winter. Mon Weather Rev 141(4):1347–1357
Gonzalez AO, Jiang X (2019) Distinct propagation characteristics of intraseasonal variability over the tropical west Pacific. J Geophys Res Atmos 124(10):5332–5351
Hersbach H et al (2020) The ERA5 global reanalysis. Quart J R Meteoro Soc 146(730):1999–2049
Huang P, Huang R (2011) Climatology and interannual variability of convectively coupled equatorial waves activity. J Clim 24:4451–4465
Huang K, Pegion K (2022) The roles of westward-propagating waves and the QBO in limiting MJO propagation. J Clim 35(18):6031–6049
Huang B et al (2017) Extended reconstructed sea surface temperature, version 5 (ERSSTv5): upgrades, validations, and intercomparisons. J Clim 30(20):8179–8205
Hsu PC, Li T (2012) Role of the boundary layer moisture asymmetry in causing the eastward propagation of the Madden–Julian oscillation. J Clim 25(14):4914–4931
Jiang X et al (2015) Vertical structure and physical processes of the Madden-Julian oscillation: exploring key model physics in climate simulations. J Geophys Res Atmos 120:4718–4748
Karmakar N, Misra V (2020) Differences in northward propagation of convection over the Arabian Sea and Bay of Bengal during boreal summer. J Geophys Res Atmos 125(3):e2019JD031648. https://doi.org/10.1029/2019JD031648
Kikuchi K (2021) The Boreal Summer Intraseasonal Oscillation (BSISO): a review. J Meteorol Soc Jpn. https://doi.org/10.2151/jmsj.2021045
Kiladis GN, Wheeler MC (1995) Horizontal and vertical structure of observed tropospheric equatorial Rossby waves. J Geophys Res Atmos 100(D11):22981–22997
Kiladis GN, Wheeler MC, Haertel PT, Straub KH, Roundy PE (2009) Convectively coupled equatorial waves. Rev Geophys. https://doi.org/10.1029/2008rg000266
Kiladis GN et al (2014) A comparison of OLR and circulation-based indices for tracking the MJO. Mon Weather Rev 142(5):1697–1715
Kim JE, Zhang C (2021) Core dynamics of the MJO. J Atmos Sci 78:229–248
Kim D et al (2009) Application of MJO simulation diagnostics to climate models. J Clim 22(23):6413–6436
Kim HM et al (2016) MJO Propagation across the maritime continent in the ECMWF ensemble prediction system. J Clim 29(11):3973–3988
Kim HM et al (2019) MJO propagation processes and mean biases in the SubX and S2S reforecasts. J Geophys Res Atmos 124(16):9314–9331
Komaromi WA, Coauthors, (2019) Examining the predictability of the successive MJO events of November 2011 using coupled 30-Day NAVGEM and COAMPS simulations. Mon Weather Rev 147(6):2123–2143
Konda G, Vissa NK (2022) Robustness of BSISO and air-sea interactions in the CMIP (Phase-6) models over the North Indian Ocean. Dyn Atmos Ocean 99:101316. https://doi.org/10.1016/j.dynatmoce.2022.101316
Le P et al (2021) Underestimated MJO variability in CMIP6 models. Geophys Res Lett 48(12):e2020GL092244. https://doi.org/10.1029/2020gl092244
Li K et al (2022) Maintenance of the basin-dependent quasi-biweekly mode in the Indian Ocean during summer. J Clim 35(11):3587–3601
Liebmann B, Smith CA (1996) Description of a complete (interpolated) outgoing longwave radiation dataset. Bull Am Meteorol Soc 77(6):1275–1277
Ling J, Zhang C, Joyce R, Xie PP, Chen G (2019) Possible role of the diurnal cycle in land convection in the barrier effect on the MJO by the Maritime Continent. Geophys Res Lett 46(5):3001–3011
Liu F, Li T, Wang H, Deng L, Zhang Y (2016) Modulation of boreal summer intraseasonal oscillations over the western North Pacific by ENSO. J Clim 29(20):7189–7201
Madden RA (1986) Seasonal variations of the 40–50 day oscillation in the tropics. J Atmos Sci 43(24):3138–3158
Madden RA, Julian PR (1971) Detection of a 40–50 day oscillation in the zonal wind in the tropical Pacific. J Atmos Sci 28:702–708
Madden RA, Julian PR (1972) Description of global-scale circulation cells in the tropics with a 40–50 day period. J Atmos Sci 29(6):1109–1123
Majda AJ, Stechmann SN (2009) The skeleton of tropical intraseasonal oscillations. Proc Natl Acad Sci 106(21):8417–8422
Majda AJ, Stechmann SN (2011) Nonlinear dynamics and regional variations in the MJO skeleton. J Atmos Sci 68:3053–3071
Mamidi K, Mathew V (2023) Minimal mechanisms responsible for the dispersive behavior of the Madden–Julian oscillation. Climate 11:236. https://doi.org/10.3390/cli11120236
Martin Z et al (2021) The influence of the quasi-biennial oscillation on the Madden–Julian oscillation. Nat Rev Earth Environ 2:477–489
Masunaga H (2007) Seasonality and regionality of the Madden-Julian oscillation, kelvin wave, and equatorial Rossby wave. J Atmos Sci 64:4400–4416
Matsuno T (1966) Quasi-geostrophic motions in the equatorial area. J Meteorol Soc Japan 44:25–43
Matthews AJ (2008) Primary and successive events in the Madden–Julian oscillation. Q J R Meteorol Soc 134:439–453
Mayta VC, Adames ÁF (2023) Is the Madden-Julian oscillation a moisture mode? Geophys Res Lett 50:e2023GL103002. https://doi.org/10.22541/essoar.167590828.80751158/v1
Mayta VC, Adames ÁF, Ahmed F (2022) Westward-propagating moisture mode over the tropical western hemisphere. Geophys Res Lett 49(6):e2022GL097799. https://doi.org/10.1029/2022gl097799
Mu M, Duan WS, Wang B (2003) Conditional nonlinear optimal perturbation and its applications. Nonlinear Process Geophys 10(6):493–501
Nakamura Y, Takayabu YN (2022) Convective couplings with equatorial Rossby waves and equatorial Kelvin waves. Part I: coupled wave structures. J Atmos Sci 79(1):247–262
Neena JM, Lee JY, Waliser D, Wang B, Jiang X (2014) Predictability of the Madden–Julian oscillation in the intraseasonal variability hindcast experiment (ISVHE). J Clim 27(12):4531–4543
Neena JM, Lee JY, Waliser D, Jiang X (2017) Model performance metrics and process diagnostics for boreal summer intraseasonal variability. Clim Dyn 48:1661–1683
Ren HL, Wei Y, Zhao S (2023) Low-frequency variability in the real-time multivariate MJO index: real or artificial? J Clim 36(7):2073–2089

Rostami N, Zhao B, Petri S (2022) On the genesis and dynamics of Madden–Julian oscillation-like structure formed by equatorial adjustment of localized heating. Q J R Meteorol Soc. https://doi.org/10.1002/qj.4388
Roundy P (2023) Equatorial Rossby waves and their impacts on monsoon region deep convection. Mausam 74(2):267–272
Roundy P, Frank W (2004a) Applications of a multiple linear regression model to the analysis of relationships between eastward- and westward-moving intraseasonal modes. J Atmos Sci 61(24):3041–3048
Roundy P, Frank W (2004b) Effects of low-frequency wave interactions on intraseasonal oscillations. J Atmos Sci 61(24):3025–3040
Slingo J et al (1999) On the predictability of the interannual behavior of the Madden-Julian Oscillation and its relationship with El Niño. Q J R Meteorol Soc 125:583–609
Sobel A, Maloney ED (2013) Moisture modes and the eastward propagation of the MJO. J Atmos Sci 70:187–192
Sobel A et al (2008) The role of surface heat fluxes in tropical intraseasonal oscillations. Nature Geosci 1:653–657
Straub KH (2013) MJO initiation in the real-time multivariate MJO index. J Clim 26(4):1130–1151
Takasuka D, Satoh M (2021) Diversity of the Madden–Julian oscillation: Initiation region modulated by the interaction between the intraseasonal and interannual variabilities. J Clim 34(6):2297–2318
Waliser DE, Lau KM, Stern W, Jones C (2003) Potential predictability of the Madden–Julian oscillation. Bull Amer Meteor Soc 84(1):33–50
Waliser DE et al (2009) MJO simulation diagnostics. J Clim 22(11):3006–3030
Wang L, Chen L (2016) Interannual variation of convectively-coupled equatorial waves and their association with environmental factors. Dyn Atmos Ocean 76:116–126
Wang B, Rui H (1990) Synoptic climatology of transient tropical intraseasonal convection anomalies: 1975–1985. Meteorol Atmos Phys 44:43–61
Wang S, Sobel AH (2022) A unified moisture mode theory for the Madden–Julian oscillation and the boreal summer intraseasonal oscillation. J Clim 35(4):1267–1291
Wang B, Xie X (1996) Low-frequency equatorial waves in vertically sheared zonal flow. Part I: stable waves. J Atmos Sci 53(3):449–467
Wang B, Xie X (1997) A model for the boreal summer intraseasonal oscillation. J Atmos Sci 54(1):72–86
Wang B, Liu F, Chen G (2016) A trio-interaction theory for Madden–Julian oscillation. Geosci Lett 3:1–16
Wang B, Chen G, Liu F (2019) Diversity of the Madden-Julian oscillation. Sci Adv 5(7):eaax0220. https://doi.org/10.1126/sciadv.aax0220
Wang S, Tan Z-M, Wu Z, Fang F (2022) Moisture modes of tropical intraseasonal oscillations—high order and anti-symmetric solutions. J Geophys Res Atmos 127:e2021JD036413. https://doi.org/10.1029/2021JD036413
Wang Y, Ren HL, Wei Y, Wu J, Zhao S (2024). MJO Initiation Westward Shifted and Propagation Blocked under Indian Ocean Basin Warming during Boreal Summer. https://doi.org/10.22541/essoar.171352180.04827554/v1
Wei Y, Ren HL (2019) Modulation of ENSO on fast and slow MJO modes during boreal winter. J Clim 32(21):7483–7506
Wei Y, Ren HL (2024) MJO seasonality in its scale selection: perspectives from space-time spectral analysis of moisture budget. J Geophys Res Atmos. https://doi.org/10.1029/2023JD039645
Wei Y, Mu M, Ren HL, Fu JX (2019) Conditional nonlinear optimal perturbations of moisture triggering primary MJO initiation. Geophys Res Lett 46:3492–3501
Wei Y, Ren HL, Mu M, Fu JX (2020) Nonlinear optimal moisture perturbations as excitation of primary MJO events in a hybrid coupled climate model. Clim Dyn 54:675–699
Wei Y, Liu F, Ren HL et al (2022) Western Pacific premoistening for eastward-propagating BSISO and its ENSO modulation. J Clim 35(15):4979–4996
Wei Y, Ren HL, Xiang B, Wang Y, Wu J, Wang S (2023a) Diverse MJO genesis and predictability. Bull Amer Meteor Soc 104(4):E792–E809
Wei Y, Ren HL, Duan W, Sun G (2023b) Westward-propagating disturbances shape diverse MJO propagation. Geophys Res Lett 50(17):e2023GL104778. https://doi.org/10.1029/2023gl104778
Wheeler MC, Hendon H (2004) An all-season real-time multivariate MJO index: development of an index for monitoring and prediction. Mon Wea Rev 132:1917–1932
Wheeler MC, Kiladis GN (1999) Convectively coupled equatorial waves: Analysis of clouds and temperature in the wavenumber–frequency domain. J Atmos Sci 56:374–399
Wheeler MC, Kiladis GN, Webster PJ (2000) Large-scale dynamical fields associated with convectively coupled equatorial waves. J Atmos Sci 57(5):613–640
Xie X, Wang B (1996) Low-frequency equatorial waves in vertically sheared zonal flow. Part II: unstable waves. J Atmos Sci 53(23):3589–3605
Yang D, Ingersoll AP (2013) Triggered convection, gravity waves, and the MJO: a shallow-water model. J Atmos Sci 70(8):2476–2486
Yang D, Ingersoll AP (2014) A theory of the MJO horizontal scale. Geophys Res Lett 41(3):1059–1064
Yang GY, Hoskins B, Slingo J (2007a) Convectively coupled equatorial waves. Part I: horizontal and vertical structures. J Atmos Sci 64(10):3406–3423
Yang GY, Hoskins B, Slingo J (2007b) Convectively coupled equatorial waves. Part II: propagation characteristics. J Atmos Sci 64(10):3424–3437
Yang GY, Hoskins B, Slingo J (2016) ENSO-related variation of equatorial MRG and Rossby waves and forcing from higher latitudes. Q J R Meteorol Soc 142:2488–2504
Yasunaga K (2011) Seasonality and regionality of the Madden-Julian oscillation and convectively coupled equatorial waves. SOLA 7:153–156
Zhang C (2005) Madden-Julian oscillation. Rev Geophys 43(2):RG2003. https://doi.org/10.1029/2004rg000158
Zhang C (2013) Madden–Julian oscillation: bridging weather and climate. Bull Am Meteorol Soc 94(12):1849–1870
Zhang C, Dong M (2004) Seasonality in the Madden–Julian oscillation. J Clim 17:3169–3180
Zhang C, Hendon HH (1997) Propagating and standing components of the intraseasonal oscillation in tropical convection. J Atmos Sci 54(6):741–752
Zhang C, Ling J (2017) Barrier effect of the Indo-Pacific Maritime Continent on the MJO: perspectives from tracking MJO precipitation. J Clim 30:3439–3459
Zhang C, Adames ÁF, Khouider B, Wang B, Yang D (2020) Four theories of the Madden-Julian oscillation. Rev Geophys 58(3):e2019RG000685. https://doi.org/10.1029/2019rg000685

Publisher's Note Springer Nature remains neutral with regard to jurisdictional claims in published maps and institutional affiliations.

Springer Nature or its licensor (e.g. a society or other partner) holds exclusive rights to this article under a publishing agreement with the author(s) or other rightsholder(s); author self-archiving of the accepted manuscript version of this article is solely governed by the terms of such publishing agreement and applicable law.